ACCOUNTS of chemical research

pubs.acs.org/accounts Article

Solvation and Mobilization of Copper Active Sites in Zeolites by Ammonia: Consequences for the Catalytic Reduction of Nitrogen Oxides

Christopher Paolucci, John R. Di Iorio, William F. Schneider,* and Rajamani Gounder*

Cite This: https://dx.doi.org/10.1021/acs.accounts.0c00328 Read Online

CONSPECTUS: Copper-exchanged chabazite (Cu-CHA) zeolites are catalysts used in diesel emissions control for the abatement of nitrogen oxides (NO_x) via selective catalytic reduction (SCR) reactions with ammonia as the reductant. The discovery of these materials in the early 2010s enabled a step-change improvement in diesel emissions aftertreatment technology. Key advantages of Cu-CHA zeolites over prior materials include their effectiveness at the lower temperatures characteristic of diesel exhaust, their durability under high-temperature hydrothermal conditions, and their resistance to poisoning from residual hydrocarbons present in exhaust. Fundamental catalysis research has since uncovered mechanistic and kinetic features that underpin the ability of Cu-CHA to selectively reduce NO_x under strongly oxidizing conditions and to achieve improved NO_x conversion relative to other zeolite frameworks, particularly at low exhaust temperatures and with ammonia instead of other reductants.

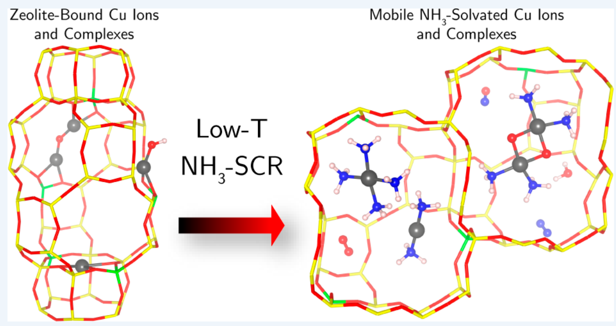

One critical mechanistic feature is the NH_3 solvation of exchanged Cu ions at low temperatures (<523 K) to create cationic Cu–amine coordination complexes that are ionically tethered to anionic Al framework sites. This ionic tethering confers regulated mobility that facilitates interconversion between mononuclear and binuclear Cu complexes, which is necessary to propagate SCR through a Cu^{2+}/Cu^{+} redox cycle during catalytic turnover. This dynamic catalytic mechanism, wherein single and dual metal sites interconvert to mediate different half-reactions of the redox cycle, combines features canonically associated with homogeneous and heterogeneous reaction mechanisms.

In this Account, we describe how a unified experimental and theoretical interrogation of Cu-CHA catalysts in operando provided quantitative evidence of regulated Cu ion mobility and its role in the SCR mechanism. This approach relied on new synthetic methods to prepare model Cu-CHA zeolites with varied active-site structures and spatial densities in order to verify that the kinetic and mechanistic models describe the catalytic behavior of a family of materials of diverse composition, and on new computational approaches to capture the active-site structure and dynamics under conditions representative of catalysis. Ex situ interrogation revealed that the Cu structure depends on the conditions for the zeolite synthesis, which influence the framework Al substitution patterns, and that statistical and electronic structure models can enumerate Cu site populations for a known Al distribution. This recognition unifies seemingly disparate spectroscopic observations and inferences regarding Cu ion structure and responses to different external conditions. SCR rates depend strongly on the Cu spatial density and zeolite composition in kinetic regimes where Cu^{+} oxidation with O_2 becomes rate-limiting, as occurs at lower temperatures and under fuel-rich conditions. Transient experiments, ab initio molecular dynamics simulations, and statistical models relate these sensitivities to the mobility constraints imposed by the CHA framework on NH_3-solvated Cu ions, which regulate the pore volume accessible to these ions and their ability to pair and complete the catalytic cycle. This highlights the key characteristics of the CHA framework that enable superior performance under low-temperature SCR reaction conditions.

This work illustrates the power of precise control over a catalytic material, simultaneous kinetic and spectroscopic interrogation over a wide range of reaction conditions, and computational strategies tailored to capture those reaction conditions to reveal in

continued...

Received: May 27, 2020

microscopic detail the mechanistic features of a complex and widely practiced catalysis. In doing so, it highlights the key role of ion mobility in catalysis and thus potentially a more general phenomenon of reactant solvation and active site mobilization in reactions catalyzed by exchanged metal ions in zeolites.

KEY REFERENCES

- Paolucci, C.; Khurana, I.; Parekh, A. A.; Li, S.; Shih, A. J.; Li, H.; Di Iorio, J. R.; Albarracin-Caballero, J. D.; Yezerets, A.; Miller, J. T.; Delgass, W. N.; Ribeiro, F. H.; Schneider, W. F.; Gounder, R. Dynamic multinuclear sites formed by mobilized copper ions in NOx selective catalytic reduction. *Science* **2017**, *357*, 898−903.[1] *The oxidation half-cycle in SCR proceeds through the transient and reversible pairing of nominally site-isolated and NH_3-solvated Cu^I ions and their reaction with O_2 in processes that are quantitatively described using non-mean-field kinetic models that reflect the regulated mobility of Cu ions conferred by ionic tethering.*
- Paolucci, C.; Parekh, A. A.; Khurana, I.; Di Iorio, J. R.; Li, H.; Caballero, J. D. A.; Shih, A. J.; Anggara, T.; Delgass, W. N.; Miller, J. T.; Ribeiro, F. H.; Gounder, R.; Schneider, W. F. Catalysis in a Cage: Condition-Dependent Speciation and Dynamics of Exchanged Cu Cations in SSZ-13 Zeolites. *J. Am. Chem. Soc.* **2016**, *138*, 6028−6048.[2] *Models are developed to predict and enumerate Cu site speciation in CHA zeolites of varying composition prepared experimentally, and exchanged Cu ions are shown to become solvated by NH_3 under SCR reaction conditions to form mobile and redox-active Cu−amine complexes confined within CHA cages.*
- Di Iorio, J. R.; Li, S.; Jones, C. B.; Nimlos, C. T.; Wang, Y.; Kunkes, E.; Vattipalli, V.; Prasad, S.; Moini, A.; Schneider, W. F.; Gounder, R. Cooperative and Competitive Occlusion of Organic and Inorganic Structure-Directing Agents within Chabazite Zeolites Influences Their Aluminum Arrangement. *J. Am. Chem. Soc.* **2020**, *142*, 4807−4819.[3] *Experiment and theory are used to study the influence of different organic and inorganic structure-directing cations on the framework Al substitution patterns formed in CHA zeolites, with resulting consequences for the speciation of exchanged Cu ions.*
- Li, H.; Paolucci, C.; Khurana, I.; Wilcox, L. N.; Göltl, F.; Albarracin-Caballero, J. D.; Shih, A. J.; Ribeiro, F. H.; Gounder, R.; Schneider, W. F. Consequences of Exchange-Site Heterogeneity and Dynamics on the UV−Visible Spectrum of Cu-Exchanged SSZ-13. *Chem. Sci.* **2019**, *10*, 2373−2384.[4] *Spectroscopic experiments on Cu-CHA samples prepared to contain majority paired and isolated Al sites combined with first-principles ensemble-averaged calculations of electronic spectra reveal the spectroscopic fingerprints of two distinct isolated Cu^{II} exchange sites, the fluxional nature of those sites, and the confounding contributions of oxygen-bridged Cu ion pairs to the observed spectra.*

1. INTRODUCTION

The active site is a foundational concept in catalysis.[5] Common structural motifs in heterogeneous catalysis are metal particles dispersed onto a nonuniform support, for which the precise identity or uniqueness of the active site is difficult to establish.[6] In the limit of single metal sites dispersed onto an oxide support (i.e., "single-atom catalysts"),[7] the envisioned active sites are distinct entities defined by coordination of the metal ion by a ligand framework provided by the support, in direct analogy to coordinated metal ions familiar to inorganic and organometallic homogeneous catalysis.[8] Metal ions substituted within or dispersed onto zeolites were early examples of purported single-site catalysts.[6,9] Zeolites are open porous crystalline frameworks built from corner-sharing oxygen tetrahedra centered by silicon and aluminum, corresponding compositionally to $(SiO_2)_x(AlO_2^-)_y$, where x/y is the silicon-to-aluminum ratio (Si/Al). To maintain charge neutrality, each AlO_2^- tetrahedral site (T-site) is charge-compensated by an extralattice ion, which can serve as an active site.

The ability of zeolites to host metal-ion active sites was recognized in the 1950s.[10] In the 1970s, Cu-exchanged zeolite Y was reported to effectively catalyze the ammonia-assisted selective catalytic reduction (NH_3-SCR) of nitrogen oxides (NO_x):[11,12]

$$4NO + 4NH_3 + O_2 \rightarrow 4N_2 + 6H_2O \quad (1)$$

Interest in Cu-exchanged zeolites surged in the 1990s with the need to address NO_x emissions from diesel engines.[13] The potential for NH_3 to solvate and even mobilize Cu ions within zeolites was noted at this time,[11] foreshadowing some surprising features of the NH_3-SCR reaction mechanism and catalytic behavior described here. In 2010, Kwak et al. reported that the NH_3-SCR catalytic performance was significantly improved by incorporation of Cu ions into the small-pore chabazite (CHA) zeolite SSZ-13 (Figure 1),[14,15] and such catalysts are now widely used for diesel NO_x emissions control.[16,17]

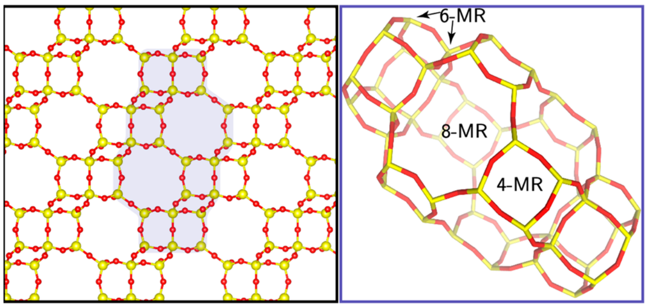

Figure 1. (left) CHA crystallographic structure and (right) the CHA cage. Adapted with permission from ref 1. Copyright 2017 American Association for the Advancement of Science.

Since Cu is low-valent and can adopt 1+ and 2+ oxidation states, its ability to associate with AlO_2^- sites within zeolites and participate in redox catalysis is unsurprising. The speciation of Cu ions, its relationship to the primary reporters of catalyst composition (Si/Al, Cu/Al), and how this relationship changes in the SCR reaction environment are less evident and an active area of research.[15] Here we summarize the relationships revealed from an integrated application of atom-precise materials synthesis, spectroscopic and kinetic characterizations performed in operando, and theoretical modeling. The resulting learnings highlight how the environment and dynamics of nominally isolated Cu ions within the CHA framework play crucial roles in determining SCR catalytic function and provide fundamental

https://dx.doi.org/10.1021/acs.accounts.0c00328
Acc. Chem. Res. XXXX, XXX, XXX−XXX

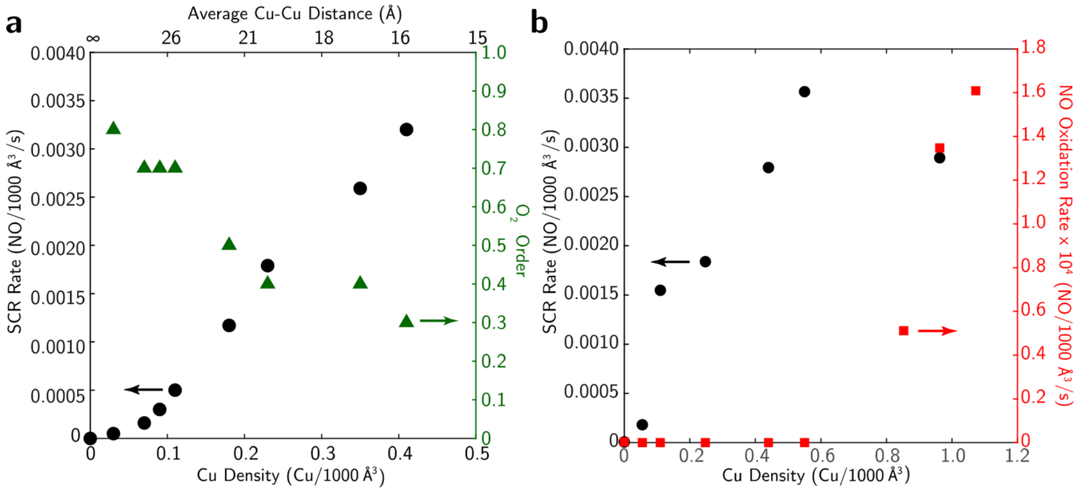

Figure 2. (a) NH_3-SCR rates (at 473 K, per unit catalyst pore volume) and apparent orders with respect to O_2 under "standard" reaction conditions (0.03 kPa NO, 0.03 kPa NH_3, 7 kPa CO_2, 10 kPa O_2, 2.5 kPa H_2O), measured on Cu-CHA (Si/Al = 15) with increasing Cu ion density. Adapted with permission from ref 1. Copyright 2017 American Association for the Advancement of Science. (b) NH_3-SCR rates (at 473 K, black) and dry NO oxidation rates (at 543 K, red; per unit catalyst pore volume, 0.032 kPa NO, 0.015 kPa NO_2, 10 kPa O_2) measured on Cu-CHA (Si/Al = 4.5) with increasing Cu content. Adapted with permission from refs 19 and 20. Copyright 2014 Elsevier.

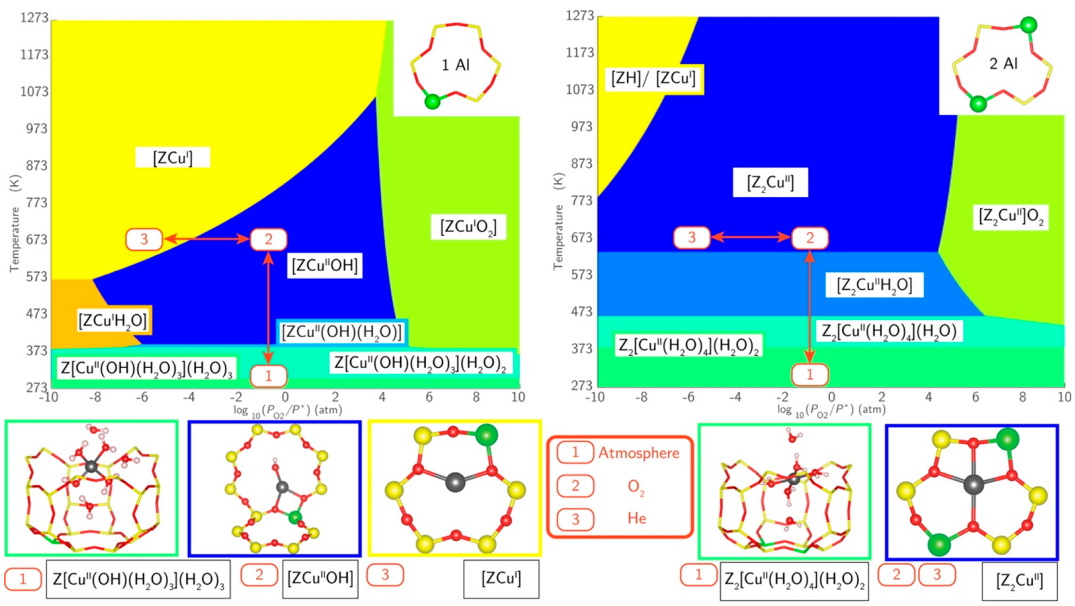

Figure 3. Ex situ Cu speciation phase diagrams (HSE06-TSvdw calculations) on (left) 1Al and (right) 2Al exchange sites. Regions indicate the site compositions that minimize the free energy at 2 kPa H_2O and the given T and P_{O_2}. Minimum free energy species under (1) ambient (298 K, 20 kPa O_2), (2) oxidizing (673 K, 20 kPa O_2), and (3) inert (673 K, 10^{-4} kPa O_2) conditions are labeled on the phase diagram and illustrated below. Reproduced from ref 2. Copyright 2016 American Chemical Society.

insights to guide new applications of mobile metal ion sites in zeolites for other reactions.

2. SCR RATES SHOW A COMPLEX DEPENDENCE ON CU-ZEOLITE COMPOSITION

The relevance of catalyst composition and reaction environment to SCR function is betrayed by reaction kinetics, even when measured under fixed conditions representative of practical low-temperature applications of the "standard" SCR reaction (eq 1). On Cu-CHA zeolites of varying composition that were prepared to contain nominally isolated Cu ions, the SCR kinetic parameters (at 473 K) depend systematically on the Cu content. As shown in Figure 2a, the SCR rate (per unit catalyst pore volume) increases quadratically with Cu density up to a volume-averaged density of 0.1 Cu/1000 Å^3 and then depends linearly on the Cu density.[1,18] Concomitantly, the apparent reaction order with respect to O_2 decreases systematically (Figure 2a) with increasing Cu content.[1] At even higher Cu densities (0.96 Cu/1000 Å^3; Figure 2b), the SCR rate on Cu-CHA decreases with increasing Cu content, coincident with the spectroscopic observation of bulk copper oxides that persist during and after the reaction.[19,20]

The dry NO oxidation ($2NO + O_2 \rightarrow 2NO_2$) rate (per unit catalyst pore volume) measured on Cu-CHA in a similar composition range follows a different pattern. The NO oxidation rate is undetectable at Cu densities less than 0.85 Cu/1000 Å^3 (Figure 2b) and then begins to increase with increasing Cu content. The NO oxidation rates (per Cu) are at least 10 times

https://dx.doi.org/10.1021/acs.accounts.0c00328
Acc. Chem. Res. XXXX, XXX, XXX−XXX

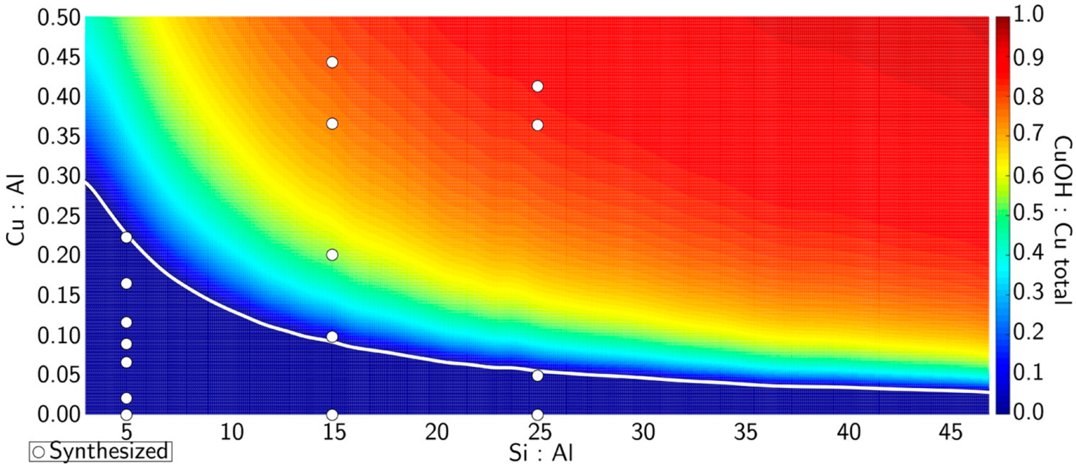

Figure 4. Predicted Cu speciation versus Si/Al and Cu/Al ratio assuming a random Al distribution (subject to Loewenstein's rule). The color scale at the right indicates the predicted fraction of ZCuOH. The white line demarcates the transition from the Z_2Cu-only region (below) to the mixed Z_2Cu/ZCuOH region (above). White circles indicate compositions of synthesized Cu-CHA samples. Reproduced from ref 2. Copyright 2016 American Chemical Society.

lower than the NH_3-SCR rates on Cu-CHA zeolites (Table S2) and are inhibited by NO_2 and H_2O, which are present during SCR catalysis. Thus, NO oxidation is irrelevant to the low-temperature NH_3-SCR reaction, as often implicated in early mechanistic proposals. NO oxidation rather appears to be associated with multinuclear Cu−oxide species[19] and thus is a useful probe reaction for these species. Taken together, these kinetic data indicate that multiple forms of Cu species exist on Cu-CHA as a function of Cu content, motivating ex situ and in operando characterization of the Cu structure and oxidation state.

3. ISOLATED CU^{2+} IONS OCCUPY TWO DISTINCT TYPES OF EXCHANGE SITES

Spectroscopic evidence suggests that two types of isolated Cu sites nominally exist in CHA, corresponding to Cu^{2+} associated with one (Figure 3, left) or two (Figure 3, right) framework Al ions. Density functional theory (DFT) augmented with first-principles thermodynamics aids in microscopic assignment of these two exchange sites. Supercell DFT calculations indicate that the energy of a Cu^{2+} ion and a local ensemble of two framework Al ions is minimized when the Al ions are at second-nearest-neighbor (2NN) and 3NN locations within the same six-membered ring (6-MR) and thus are separated by 5−6 Å (Figure S1). In these "Z_2Cu" sites, framework oxygen (O_f) provides a fourfold coordination environment, as favored by the d^9 Cu^{2+} ion. In contrast, a Cu^{2+} ion associated with an isolated Al site (i.e., 1Al site) requires an extralattice ligand (e.g., OH^-) to provide charge neutrality. The energies of the resultant "ZCuOH" sites can be computed and compared with those of Z_2Cu sites via an appropriate exchange reaction, which indicates that isolated Z_2Cu sites are 66 kJ/mol lower in energy than ZCuOH sites (Figure S2); thus, equilibrated exchange processes would cause Z_2Cu sites to become preferentially populated at 2Al sites before ZCuOH at 1Al sites.

To evaluate how Cu^{2+} sites evolve under conditions representative of catalyst preparation, dehydration, and high-temperature oxidative treatments, we applied a first-principles thermodynamics strategy.[2] We enumerated and evaluated the relative free energies of different possible Cu ion coordination states as functions of the external conditions of temperature and gas pressure, including any number of associated H_2O ligands and the corresponding Cu^+ structures expected to form upon Cu^{2+} reduction. The free energies were evaluated through annealing of candidate structures using ab initio molecular dynamics (AIMD), HSE06 energy evaluations, and finite-temperature corrections based on correlations developed from potential of mean force (PMF) simulations.[21] Figure 3 reports predicted phase diagrams for Z_2Cu and ZCuOH sites as functions of temperature and O_2 pressure at fixed H_2O pressure. The models predict that both Cu sites are hydrated under ambient conditions (Figure 3, state 1) and become dehydrated at elevated temperature in O_2 (Figure 3, state 2) and that ZCuOH sites but not Z_2Cu sites "autoreduce" to Cu^+ (ZCu) in inert environments (Figure 3, state 3). Separately, from calculations of exchange energies, the preference for populating Z_2Cu sites over ZCuOH sites is predicted to be independent of the extent of hydration.

Experimental efforts to characterize these two Cu^{2+} site types are aided by preparing Cu-CHA materials that emphasize Z_2Cu or ZCuOH motifs. Their relative population in a given zeolite depends on the number and distribution of Al ions in the framework and the Cu/Al ratio. Materials with low Si/Al and Cu/Al ratios should contain predominantly Z_2Cu sites, while materials with high Si/Al and Cu/Al ratios are dominated by ZCuOH sites. To test these predictions, we synthesized Cu-CHA with diverse composition (Table S3) and developed a suite of analytical techniques to identify and quantify Z_2Cu and ZCuOH sites after different treatment conditions, which determine the ability of experiments to differentiate Z_2Cu and ZCuOH according to the computed phase diagrams (Figure 3).

Under ambient conditions, experimental X-ray absorption spectroscopy (XAS), UV−vis, and IR spectra of Cu-CHA with varying composition are spectroscopically indistinguishable from aqueous $[Cu(H_2O)_6]^{2+}$ references,[2,19,20] consistent with the presence of H_2O-solvated Cu^{2+} and $[CuOH]^+$, as predicted by Figure 3. In contrast, Z_2Cu and ZCuOH site motifs are distinguishable in the absence of H_2O. Experimental XAS spectra of Cu-CHA treated with 20 kPa O_2 at 673 K show differences in the EXAFS region for first-shell coordination (four-coordinate Z_2Cu, three-coordinate ZCuOH), consistent with DFT-predicted molecular structures.[2] The IR spectra show OH stretching features (~3655 cm^{-1}) for materials containing

https://dx.doi.org/10.1021/acs.accounts.0c00328
Acc. Chem. Res. XXXX, XXX, XXX−XXX

ZCuOH sites but not those containing Z_2Cu.[2,22] The UV−vis spectra show splitting of the d−d transition band (10000−20000 cm^{-1}) in samples containing ZCuOH,[4,23] while this splitting is absent in those containing Z_2Cu.[4,19,24] Additionally, XAS spectra[2,22,23] collected after inert (673 K, He) or H_2 treatments (523 K, 3 kPa H_2) show reduction to Cu^+ in Cu-CHA samples containing ZCuOH sites but not in those containing Z_2Cu.[2] Finally, titrimetric methods using NH_3 to quantify residual H^+ sites on Cu-exchanged zeolites can distinguish Z_2Cu and ZCuOH site motifs because each Z_2Cu exchanges two H^+ whereas each ZCuOH exchanges only one H^+ (Figure S3).[25,26]

4. CU^{2+} SPECIATION CAN BE MODIFIED BY SYNTHESIZING CHA WITH DIFFERENT AL ARRANGEMENTS

The two distinct isolated Cu^{2+} site motifs, along with chemical response and analytical techniques to distinguish and enumerate them, provide a foundation to develop synthetic strategies to purposely modify the Al distribution in CHA frameworks as a means to influence the Cu speciation. Figure 4 shows a composition phase diagram computed with the assumptions that Al is distributed randomly but avoids first-nearest-neighbor sites (Al−O−Al; Loewenstein's rule[27]) and that Cu^{2+} ions populate 2Al sites (white line) prior to 1Al sites.[2] Our early experiments on Cu-CHA with varying Si/Al (4.5, 15, 25) and nominally random Al distributions showed spectroscopic and titration data that were consistent with model predictions (Figure 4).[2] These observations raised the question as to whether random Al distributions (subject to Loewenstein's rule) were an intrinsic feature of CHA frameworks, perhaps because it contains one unique T site, or whether the Al distribution could be an independently varied property of CHA.

To answer this question, we synthesized CHA zeolites with varying amounts of organic and inorganic structure-directing agents (SDAs) of different charge density and quantified the numbers of 2Al sites by their selective titration with Co^{2+} cations.[3] The number of 2Al sites increases on average with the bulk Al content[28] (Figure 4, white line) but also at fixed Al content when the organic SDA is replaced with certain types of inorganic SDAs.[29] When the sole SDA used to induce crystallization is *N*,*N*,*N*-trimethyl-1-adamantylammonium ($TMAda^+$), a bulky organic cation that occupies each CHA cage, the resulting CHA materials (Si/Al = 15) contain undetectable amounts of 2Al sites.[29,30] When $TMAda^+$ is partially replaced with Na^+, a cation with higher charge density that can co-occlude (in adjacent 6-MRs) with $TMAda^+$ in each CHA cage, the resulting CHA materials are of similar composition (Si/Al = 15; other synthesis conditions held constant) but contain 2Al sites that increase in proportion to the amount of Na^+ co-occluded in the crystalline products (Figure 5).[3,29,30] In contrast, when $TMAda^+$ is partially replaced with K^+, which competes for occupancy within CHA cage units, the resulting CHA materials contain virtually no 2Al sites.[3] Thus, the structures and relative amounts of organic and inorganic SDAs that crystallize CHA zeolites influence their framework Al distribution and in turn the speciation of Z_2Cu and ZCuOH sites, even at fixed composition (Si/Al, Cu/Al).

The composition phase diagram in Figure 4 accurately describes Cu-CHA materials with a random Al distribution, but synthetic protocols can bias the framework Al distribution away from that expected from random Al substitution. The Cu site population diagrams for CHA samples with nonrandom framework Al distributions look markedly different than the model shown in Figure 4. For example, a CHA zeolite synthesized using only $TMAda^+$ would nominally contain no 2Al sites (Figure 5), and the white line denoting saturation of Z_2Cu sites would be a horizontal line coincident with the *x* axis (Cu/Al = 0) in Figure 4.

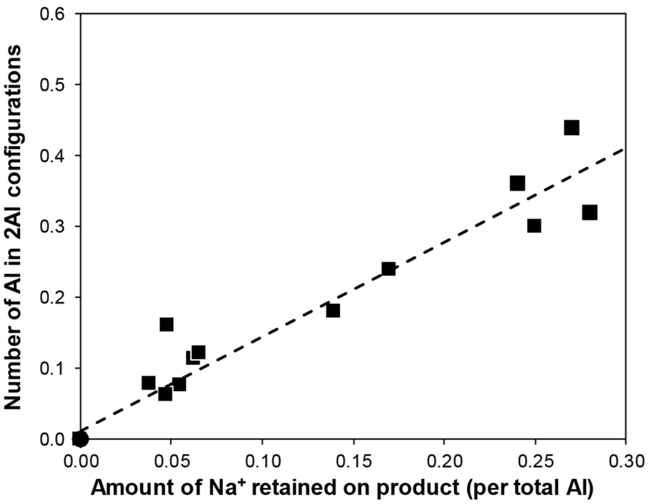

Figure 5. The number of Al in 2Al configurations (as measured by Co^{2+} titration) increases with the retained Na^+ content on CHA synthesized using $TMAda^+$ and Na^+. Adapted from ref 3. Copyright 2020 American Chemical Society.

5. CONDITION-DEPENDENT INTERCONVERSION BETWEEN MONONUCLEAR AND BINUCLEAR CU COMPLEXES

Cu-CHA materials purposely synthesized to contain either Z_2Cu or ZCuOH sites reveal that ZCuOH sites interconvert between mononuclear and binuclear structures in response to the chemical environment. The black lines in Figure 6 show UV−vis spectra of Cu-CHA materials after high-temperature oxidative treatment (673 K, 20 kPa O_2). The Z_2Cu sample shows a broad band from 7000 to 20000 cm^{-1} (d−d) and another from 25000 to 50000 cm^{-1} (ligand-to-metal charge transfer, LMCT).[4,24] These features are consistent with the absorption spectra of Z_2Cu structures computed using time-dependent DFT (TD-DFT), but only after averaging of the computed spectra of static structures sampled at intervals during AIMD simulation of Z_2Cu structures in order to account for thermally induced restructuring of Cu ions in the 6-MRs containing 2Al.[4] Thus, even when bound to the zeolite framework, Cu ions undergo significant dynamic restructuring that must be properly described to equate computed and experimental spectra.

Cu-CHA samples containing nominally ZCuOH show four features in the d−d region and a shoulder in the LMCT region around 27000 cm^{-1} in addition to the symmetric band from 25000 to 50000 cm^{-1} (Figure 6b,c). Different relative intensities are observed in the d−d region for the two Cu-CHA materials with different ZCuOH contents (Figure 6b,c) and among materials reported in the literature prepared using synthetic protocols expected to result in majority ZCuOH.[4,23,31−34] AIMD and TD-DFT-computed spectra for ZCuOH contain only two absorption features in the d−d region, inconsistent with experimentally measured spectra (Figure 6b,c). Thus, nominally ZCuOH-containing Cu-CHA materials (1Al) show

https://dx.doi.org/10.1021/acs.accounts.0c00328
Acc. Chem. Res. XXXX, XXX, XXX−XXX

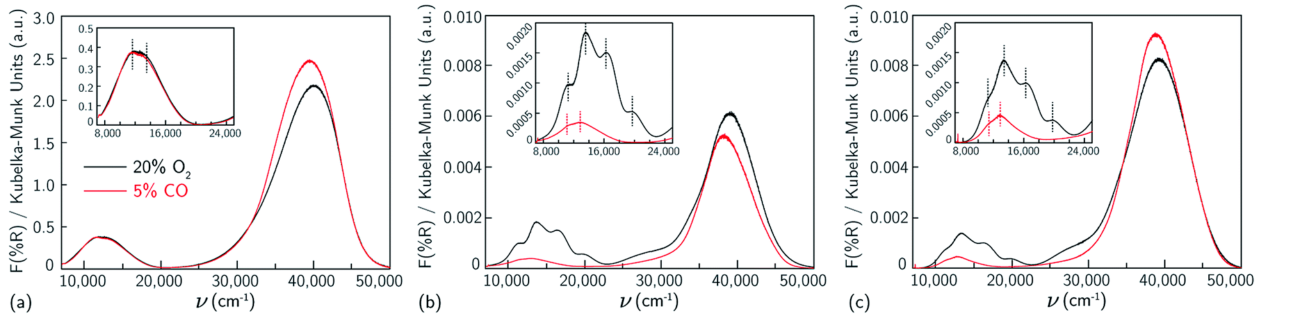

Figure 6. UV−vis spectra (at 300 K) of samples containing predominantly (a) Z_2Cu (Si/Al = 5, Cu/Al = 0.21), (b) ZCuOH (Si/Al = 15, Cu/Al = 0.24), and (c) ZCuOH (Si/Al = 15, Cu/Al = 0.15) after 20% O_2 treatment at 673 K (black) and 5% CO treatment at 523 K (red). Insets magnify the d−d transition region. From ref 4. CC BY-NC 3.0.

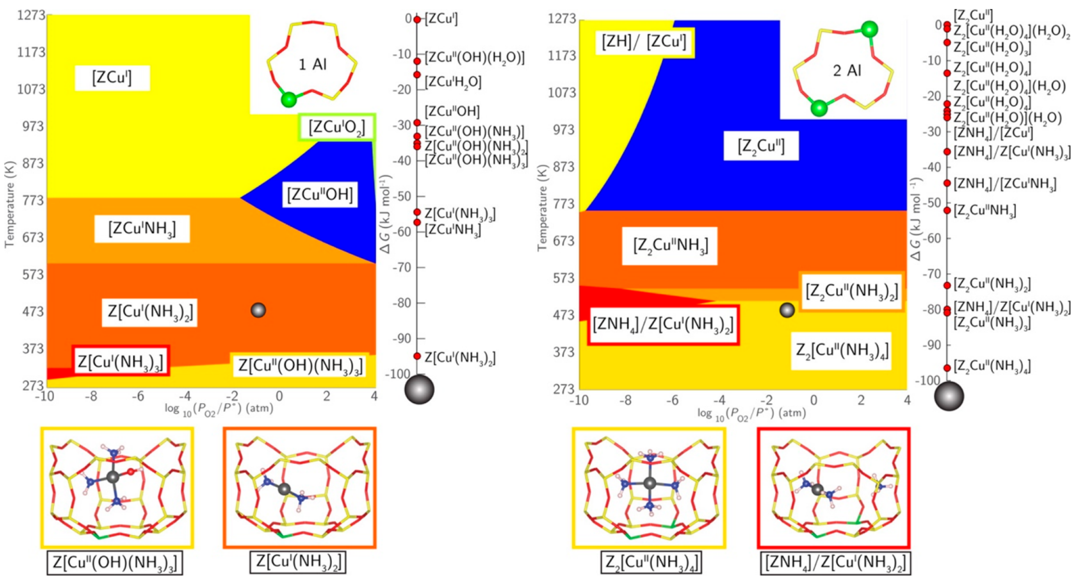

Figure 7. Phase diagrams for (left) 1Al and (right) 2Al sites with varying T and P_{O_2} at 0.030 kPa NH_3 and 2 kPa H_2O. Relative rankings for all species ($\Delta G_{form} < 0$) at 473 K and 10 kPa O_2 (chrome spheres) are to the right of each diagram. The most stable Cu^+ (red) and Cu^{2+} (gold) structures under these conditions are shown below. Reproduced from ref 2. Copyright 2016 American Chemical Society.

heterogeneous features in UV−vis spectra that computations are unable to assign solely to ZCuOH.

Reactivity data from stoichiometric reactions of O_2, CH_4, and H_2O[31,32,35−38] and catalytic dry NO oxidation[19] in addition to Raman spectra collected under dry oxidizing conditions on similar Cu-CHA materials[31,34,37] implicate the coexistence of dimers or higher-nuclearity Cu clusters alongside ZCuOH. To identify the multinuclear Cu clusters, we exposed Cu-CHA to CO (Figure 6, red lines) to consume bridging O in Cu−oxide species,[39] which would reduce Cu^{2+} to Cu^+ and cause the Cu^{2+} d−d transition to disappear. The UV−vis spectra for the Z_2Cu sample showed no changes after CO reduction, while those for ZCuOH samples showed substantial decreases in all four features in the d−d transition band, with two of them vanishing along with the shoulder at 27000 cm^{-1}. The spectra after CO treatment (Figure 6b,c) are consistent with the computed ZCuOH spectra (after accounting for site dynamics);[4] thus, the additional features arise from multinuclear Cu−oxide clusters. TD-DFT and spectral averaging methods were used to compute UV−vis spectra for candidate $Cu_2O_xH_y$ molecular models, but the spectra of distinct site motifs contain common features; DFT thus could not resolve the precise origin of the experimentally observed UV−vis features.[4]

Our results and UV−vis and Raman data from others[31,37,40] support the coexistence of dimers or higher-nuclearity Cu−oxide clusters on ZCuOH-containing Cu-CHA materials after high-temperature oxidizing treatments. Importantly, the variability of binuclear Cu site motifs formed depends on the sample composition and treatment conditions, and these sites can be reversibly transformed to mononuclear Cu^{2+} upon low-temperature exposure to H_2O (<473 K) or NH_3 (<523 K).[19,23,38,41−43] DFT calculations and experimental results indicate that H_2O and NH_3 can react with multinuclear Cu clusters to form isolated Cu structures and then solvate them to form mononuclear Cu coordination complexes.[2,41,42,44] Thus, the Cu speciation present ex situ under high-temperature oxidizing conditions is irrelevant to low-temperature (<523 K) NH_3-SCR catalysis, motivating the need to perform characterization in operando to gain insight into the SCR mechanism.[45]

6. THE SCR REDOX CYCLE INVOLVES NO AND NH_3 SERVING AS COREDUCTANTS OF Cu^{2+} TO Cu^+

Early ex situ experiments and DFT calculations identified a four-coordinate NH_3-solvated Cu^{2+} ion as one of the primary NH_3 storage sites in Cu-CHA.[46] We performed XAS experiments in operando on Cu-CHA catalysts and found Cu to be present both

https://dx.doi.org/10.1021/acs.accounts.0c00328
Acc. Chem. Res. XXXX, XXX, XXX−XXX

as four-coordinate Cu^{2+} and two-coordinate Cu^+ ions.[2,47] We used DFT and ab initio thermodynamic modeling to describe the coordination of Cu under these conditions, which revealed that under low-temperature (<523 K) NH_3-SCR conditions (a) both Cu^{2+} and Cu^+ sites are NH_3-solvated, liberated from the zeolite lattice, and highly mobile (Figure 7); (b) the first-shell coordination of these Cu−amine complexes is consistent with that observed experimentally by EXAFS of Cu-CHA[2,42,48,49] and aqueous Cu−amine complexes;[43,50,51] and (c) the Gibbs free energies of these Cu−amine complexes suggest that they are a feasible redox couple (Figure 7). Collectively, these results imply that NH_3-solvated Cu^{2+} and Cu^+ ions are reactive intermediates in the SCR redox cycle.[2]

To isolate the species that participate in the reduction half-cycle, we performed cutoff experiments in which one reactant (NH_3, NO, or O_2) was removed from the SCR reactant mixture at a time while the evolution of the Cu^{2+} and Cu^+ oxidation states was monitored by X-ray absorption near-edge structure (XANES).[47] These and our subsequent[2,52] experiments revealed that both Z_2Cu and ZCuOH are rapidly reduced to their Cu^+ states in the presence of mixtures of NO and NH_3[52] according to

$$NO + NH_3 \rightarrow N_2 + H_2O + H^+ + e^- \qquad (2)$$

DFT calculations identified a reduction pathway in which N−N bond formation is coupled to N−H bond cleavage with computed barriers that are similar for Z_2Cu and ZCuOH,[2] implying that they should be reduced at similar rates in NO and NH_3. Consistent with our calculations, the Cu^{2+} reduction rates in NO and NH_3 have a first-order dependence on the Cu density and reduction rate constants that are insensitive to the Cu density and the relative proportions of Z_2Cu and ZCuOH.[52,53] The electron in eq 2 effects reduction of Cu^{2+} to Cu^+ while the proton is accommodated by transfer to a nearby oxygen, either a lattice oxygen (in the case of Z_2Cu), whose protons can be quantified by NH_3 titration,[2,25] or a hydroxide ligand (in the case of ZCuOH) that is rejected as H_2O.[2] These results suggest that the two Cu^{2+} site types are equally reactive and thus that the SCR rates should be strictly proportional to the Cu^{2+} content. As discussed next, however, the dependence of the SCR rate on the Cu content is more complex than that expected if Cu^{2+} reduction were the sole rate-determining step in the mechanism.

7. DIMERIC CU COMPLEXES ARE INTERMEDIATES IN THE OXIDATION OF CU$^+$ TO CU^{2+}

The SCR rate on Cu-CHA (Figure 2a) increases quadratically with the Cu density at low densities (<0.1 Cu/1000 Å^3) but linearly with the Cu density at high densities (>0.19 Cu/1000 Å^3).[1,18,20,54] Operando XAS revealed that predominantly isolated Cu^+ is present in the second-order kinetic regime. Thus, second-order rate dependences on the Cu density reflect the kinetics of Cu^+ oxidation, implicating the oxidation of two Cu^+ ions with O_2. We used transient XAS experiments to monitor changes in the Cu oxidation state when NH_3-solvated Cu^+ was exposed to O_2. The O_2-assisted oxidation rate of $Cu^+(NH_3)_2$ shows a second-order dependence on the Cu density, and the Cu^+ fraction that is oxidized by O_2 depends on the Cu density (Figure 8).[1] These observations are consistent with an O_2-assisted oxidation reaction of two $Cu^+(NH_3)_2$ species:

$$2Cu^+(NH_3)_2 + O_2 \rightarrow [(H_3N)_2Cu^{2+}O_2Cu^{2+}(NH_3)_2]^{2+} \qquad (3)$$

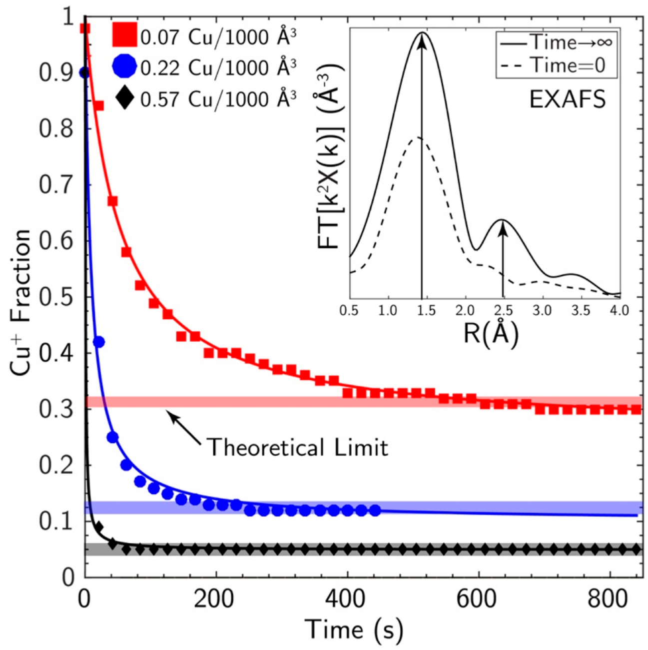

Figure 8. Cu^+ fraction during transient O_2-assisted oxidation (473 K, 10 kPa O_2) of reduced Cu-CHA samples (0.07 Cu/1000 Å^3 (red ■), 0.22 Cu/1000 Å^3 (blue ●), and 0.57 Cu/1000 Å^3 (black ♦)). Solid lines represent regression of data to a second-order Cu^+ oxidation rate equation (eq S2). Horizontal bars denote predicted recalcitrant Cu^+ fractions (Figure S4). Inset: Fourier transform of the k^2-weighted EXAFS spectrum (FT[$k^2\chi(k)$]) in R space (R) of the 0.57 Cu/1000 Å^3 sample collected before and after O_2 exposure (details in Table S4). Adapted with permission from ref 1. Copyright 2017 American Association for the Advancement of Science.

In addition to these operando and transient XAS experiments, our AIMD simulations suggest that $Cu^+(NH_3)_2$ ions are sufficiently mobile to travel between adjacent CHA cages and react with O_2 to form dimeric structures, consistent with the EXAFS spectrum measured at the end of the transient O_2 oxidation of Cu-CHA, which shows evidence of second-shell Cu−Cu scatter (Figure 8 inset).[1,55] We used metadynamics simulations to reveal that the free energy of $Cu^+(NH_3)_2$ ions increases with increasing distance to their charge-compensating framework Al centers, with a functional dependence largely described by Coulombic interactions.[1] Thus, $Cu^+(NH_3)_2$ ions are electrostatically tethered to lattice Al atoms, and two $Cu^+(NH_3)_2$ ions can participate in an O_2-assisted oxidation step (eq 3) only if they are present within distances accessible by diffusion (within ~18 Å of another Cu^+; Figures S4 and S5) on time scales relevant to steady-state turnover.[1] As a result, only a subset of Cu ions participate in the oxidation half-cycle at a given Cu density (Figure 9, central path). First-principles and stochastic simulations support the ability of two $Cu^+(NH_3)_2$ ions to react with O_2 and can successfully predict the fraction of $Cu^+(NH_3)_2$ ions that can participate in this reaction (Figure 8).[1]

These results reveal a heretofore unrecognized active-site motif involving isolated and paired metal ions that dynamically interconvert at steady state, in which single Cu ions catalyze the reduction SCR half-cycle while Cu ion pairs catalyze the oxidation SCR half-cycle. Consequently, the SCR rate and the distribution of Cu^{2+}/Cu^+ oxidation states depend on both the Cu density (Figure 2a) and the SCR reaction conditions, with Cu^+ oxidation becoming the dominant rate-limiting step at low O_2 pressures on Cu-CHA regardless of the Cu density (Figure

https://dx.doi.org/10.1021/acs.accounts.0c00328
Acc. Chem. Res. XXXX, XXX, XXX−XXX

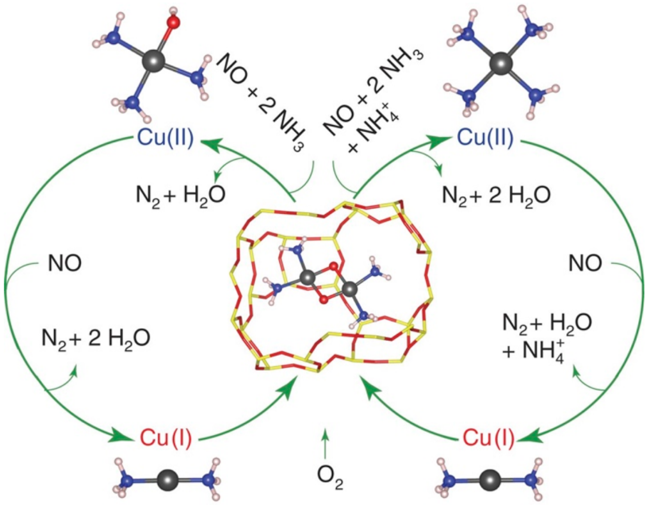

Figure 9. Proposed low-temperature SCR catalytic cycle. Reduction steps proceed on site-isolated Cu^{2+} ions residing near one (left-hand cycle) or two (right-hand cycle) framework Al ions with regulated diffusion of two Cu^+ ions into one CHA cage and oxidation by O_2 (inner step). NH_4^+ is formed and consumed in the right-hand cycle to maintain stoichiometry and charge balance. Atom colors: gray, Cu; yellow, Si; red, O; blue, N; white, H. Reproduced with permission from ref 1. Copyright 2017 American Association for the Advancement of Science.

S6).[52] Our results demonstrate that O_2-assisted oxidation steps on Cu ion pairs prevail in all Cu-CHA zeolites[52] and that the kinetic relevance of the oxidation half-cycle rate to the overall SCR rate depends on both the Cu density and O_2 partial pressure.

For Cu-CHA with compositions (Si/Al ≈ 15, Cu/Al ≈ 0.5) and low-temperature reaction conditions (<523 K, ∼5−20 kPa O_2) typical of practical steady-state SCR applications, an approximately equimolar distribution of Cu^{2+} and Cu^+ oxidation states are measured in operando by XAS,[1] indicating that both the reduction and oxidation half-cycles are kinetically relevant.

8. OUTLOOK

Experimental and theoretical assessments reveal that nominally "single-site" Cu-CHA catalysts contain a distribution of Cu site motifs, depending on the number and arrangement of Al ions in the zeolite framework and on the chemical environment. Additional spectroscopic and probe-reaction-based approaches have emerged[56−59] to quantify distinct Cu site motifs, yet they leave unresolved details for future inquiry. Under dry oxidizing conditions, how the structures and distribution of multinuclear Cu sites vary with zeolite composition and synthesis protocol is unknown but relevant to other reactions such as methane oxidation to methanol.[38,60−63] Zeolite synthesis to bias framework Al and Cu site motifs,[3,29,30] combined with the calculation of spectral features that capture dynamic Cu restructuring at finite temperatures,[4] can help more accurately identify multinuclear sites. This presents new synthetic opportunities, even for CHA, to exercise and verify control of framework Al proximity beyond distances in a 6-MR.[3,64−66] For topologies more complex than CHA, the development of experimental and computational methods to enumerate Al and Cu site types is challenging because of the combinatorial complexity associated with multiple T sites and remains an important area of research.[64]

Interrogating catalytic function over widely varying catalyst compositions and reaction conditions has revealed that the NH_3-SCR kinetics are sensitive to the metal ion proximity via steps requiring the cooperative participation of more than one metal site. However, several questions remain regarding the low-temperature NH_3-SCR mechanism. Although an NH_3-solvated Cu_2O_2 dimer is an accepted intermediate in the oxidation half-cycle,[1,18,53,58,67,68] the exact structure of the complex relevant to steady-state turnover is challenging to identify by experiment or computation.[69−71] Furthermore, the elementary steps that decompose this Cu_2O_2 species to close the SCR cycle remain unknown. Many intermediates (including NH_3-solvated Cu−nitrosyl complexes)[33,72,73] and pathways (including reactions involving HONO and H_2O and NH_4^+ species)[74−77] have been proposed, but reconciling these competing proposals may require interrogation away from "standard" SCR reaction conditions and on varying material compositions[52,78] to access regimes in which they can be kinetically discriminated.

The effects of the framework Al distribution and zeolite topology on the kinetics of different steps in the SCR cycle are also unknown, providing opportunities to quantify reduction and oxidation rate constant distributions with varying Cu density, Al density and distribution, and zeolite topology. Quantifying the fraction of Cu ions that catalyze each half-cycle requires non-mean-field kinetic models. Calculated energy differences to form Cu_2O_2 on different Al−Al pairs in CHA vary by up to 53 kJ/mol,[68] and operando data on Cu-MFI and Cu-CHA under similar conditions and compositions show different Cu^+ fractions,[79,80] motivating kinetic models sensitive to the Al distribution and zeolite topology. The SCR mechanism changes[18,38,43,54,81−83] when NH_3 desorbs from Cu at high temperatures[42,84−88] (>523 K), as multinuclear Cu sites form in the absence of NH_3 under dry oxidizing conditions;[4] however, their implications for high-temperature NH_3-SCR and unselective side reactions of NO oxidation, NH_3 oxidation, and N_2O formation are still incompletely understood. The mobility of Cu ions should also change as NH_3 becomes depleted with increasing conversion along catalyst beds or monoliths and progressively replaced by H_2O in Cu coordination spheres. Hydrated complexes (e.g., $[Cu(H_2O)_4]^{2+}$) are less mobile than NH_3-solvated Cu complexes according to AIMD,[2] and experimental characterization techniques such as electron paramagnetic resonance spectroscopy provide opportunities to probe dipolar interactions between solvated and mobile Cu^{2+} ions under hydrated conditions.[23,54]

The interrogation of Cu-CHA in operando using experiment and computation provides insights into the kinetic and mechanistic consequences of metal ion mobility, helping rationalize why Cu (metal) and NH_3 (reductant) on CHA zeolites (inorganic support) were empirically discovered as an optimal combination in the widely adopted technology for NO_x SCR. These mechanistic insights are transferrable to other methods of catalyst preparation and evolution. Treating physical mixtures of copper oxides and H-form zeolites under conditions resembling SCR enables in situ solid-state Cu ion exchange,[55,89,90] implying that pathways exist to interconvert Cu ions and oxides, the latter of which are present on commercial Cu-CHA catalysts[91] and may form during operation in potential deactivation routes.[92−95] Experimental interrogation of the mobility of Cu and other ions in zeolites includes impedance-based modulus spectroscopy with varying catalyst composition and reaction conditions.[74] Computational interrogation of ion mobility is challenging because adsorption free energies in zeolites are drastically underestimated by the standard "harmonic vibrational" assumptions that pervade the computational heterogeneous catalysis literature.[21,96−99] Metadynamics and other enhanced-sampling MD simulation techniques, which are ubiquitous for exploring complex free energy surfaces in the biological simulation community,[100] are being adapted to model reactions and species mobility in zeolites.[1,101−103] These mechanistic insights are also transferable to other chemistries, as ethene-solvated mobile Ni ions have been implicated in ethene dimerization in Ni-AFI by kinetic measurements and AIMD.[104] Moreover, H_2O-solvated Ag, Cu, Pd, and Fe sites in zeolites have been computed and observed or inferred by experiment,[2,44,87,105−107] which may provide conceptual extensions to cases wherein the molecules responsible for metal ion solvation and mobilization do not serve as reactants in the catalytic cycle. The solvation and mobilization of metal ions thus appears to be a general phenomenon of metal-zeolite catalysis under certain reaction conditions, characterized by a dynamic active-site motif that can reversibly interconvert among structures with different nuclearities to mediate distinct elementary steps during steady-state catalytic turnover.

■ ASSOCIATED CONTENT

Supporting Information

The Supporting Information is available free of charge at https://pubs.acs.org/doi/10.1021/acs.accounts.0c00328.

Supporting details mentioned in the main text (PDF)

■ AUTHOR INFORMATION

Corresponding Authors

Rajamani Gounder − *Charles D. Davidson School of Chemical Engineering, Purdue University, West Lafayette, Indiana 47907, United States;* orcid.org/0000-0003-1347-534X; Email: rgounder@purdue.edu

William F. Schneider − *Department of Chemical and Biomolecular Engineering, University of Notre Dame, Notre Dame, Indiana 46556, United States;* orcid.org/0000-0003-0664-2138; Email: wschneider@nd.edu

Authors

Christopher Paolucci − *Department of Chemical Engineering, University of Virginia, Charlottesville, Virginia 22903, United States;* orcid.org/0000-0002-4506-9306

John R. Di Iorio − *Charles D. Davidson School of Chemical Engineering, Purdue University, West Lafayette, Indiana 47907, United States;* orcid.org/0000-0002-7519-5100

Complete contact information is available at:
https://pubs.acs.org/10.1021/acs.accounts.0c00328

Author Contributions

The manuscript was written through contributions of all authors. All of the authors approved the final version of the manuscript.

Funding

We acknowledge the financial support provided by the National Science Foundation GOALI Program (Awards 1258715-CBET to J.R.D. and R.G. and 1258690-CBET to C.P. and W.F.S.). J.R.D. and R.G. also acknowledge the financial support provided by the National Science Foundation CAREER Program (Award 1552517-CBET).

Notes

The authors declare no competing financial interest.

Biographies

Christopher Paolucci is an Assistant Professor of Chemical Engineering at the University of Virginia. He received his B.S. and Ph.D. in Chemical Engineering from the University of Notre Dame in 2012 and 2017, respectively, and completed a postdoctoral appointment at Stanford University in 2018. He is a Director in the Catalysis and Reaction Engineering Division of AIChE (2019−2022). His research interests include molecular simulation and data-science-augmented approaches applied to catalyst synthesis and dynamics.

John R. Di Iorio received his B.S. in Chemical Engineering from the University of Washington in 2013 and his Ph.D. in Chemical Engineering from Purdue University in 2018. He is a postdoctoral associate at the Massachusetts Institute of Technology under the guidance of Professor Yuriy Román-Leshkov.

William F. Schneider is the Dorini Family Chair in Energy Studies and the Chair of the Department of Chemical and Biomolecular Engineering at the University of Notre Dame. He received his B.Sc. in Chemistry from the University of Michigan-Dearborn in 1986 and his Ph.D. in Chemistry from The Ohio State University in 1991, after which he joined the Ford Motor Research Laboratory. He moved to Notre Dame in 2004, where he pursues research interests in first-principles-enabled models of chemical and catalytic reactivity relevant to energy and environmental protection.

Rajamani Gounder is the Larry and Virginia Faith Associate Professor of Chemical Engineering at Purdue University. He received his B.S. in Chemical Engineering from the University of Wisconsin in 2006 and his Ph.D. in Chemical Engineering from the University of California, Berkeley in 2011 and then completed a postdoctoral appointment at the California Institute of Technology in 2013. He is the current Programming Chair and Past Director in the Catalysis and Reaction Engineering Division of AIChE (2020−2021) and was the Technical Program Co-chair of the 26th North American Catalysis Society Meeting (2019). His research interests include studying catalysis for energy and the environment, including conversion of carbon feedstocks to fuels and chemicals and automotive pollution abatement.

■ ACKNOWLEDGMENTS

We thank our collaborators who have contributed to the research discoveries described here. At Purdue, this includes Profs. Fabio Ribeiro, Nick Delgass, and Jeff Miller along with Vincent Kispersky, Shane Bates, Anuj Verma, Atish Parekh, Jonatan Albarracin-Caballero, Arthur Shih, Ishant Khurana, Trevor Lardinois, and Casey Jones. At Notre Dame, this includes Trunojoyo Anggara, Sichi Li, Hui Li, and Yujia Wang. At Cummins Inc., our long-standing collaborators and NSF/DOE GOALI partner, this includes Aleksey Yezerets and Krishna Kamasamudram and their research teams. We also acknowledge helpful technical discussions with our NSF/DOE GOALI project partners Prof. Jean-Sabin McEwen (Washington State University) and Chuck Peden, Janos Szanyi, and Feng Gao (Pacific Northwest National Laboratory). The progress described would not have been possible without the contributions of this entire group.

■ REFERENCES

(1) Paolucci, C.; Khurana, I.; Parekh, A. A.; Li, S.; Shih, A. J.; Li, H.; Di Iorio, J. R.; Albarracin-Caballero, J. D.; Yezerets, A.; Miller, J. T.; Delgass, W. N.; Ribeiro, F. H.; Schneider, W. F.; Gounder, R. Dynamic

multinuclear sites formed by mobilized copper ions in NOx selective catalytic reduction. *Science* **2017**, *357*, 898−903.
(2) Paolucci, C.; Parekh, A. A.; Khurana, I.; Di Iorio, J. R.; Li, H.; Albarracin Caballero, J. D.; Shih, A. J.; Anggara, T.; Delgass, W. N.; Miller, J. T.; Ribeiro, F. H.; Gounder, R.; Schneider, W. F. Catalysis in a Cage: Condition-Dependent Speciation and Dynamics of Exchanged Cu Cations in SSZ-13 Zeolites. *J. Am. Chem. Soc.* **2016**, *138*, 6028−6048.
(3) Di Iorio, J. R.; Li, S.; Jones, C. B.; Nimlos, C. T.; Wang, Y.; Kunkes, E.; Vattipalli, V.; Prasad, S.; Moini, A.; Schneider, W. F.; Gounder, R. Cooperative and Competitive Occlusion of Organic and Inorganic Structure-Directing Agents within Chabazite Zeolites Influences Their Aluminum Arrangement. *J. Am. Chem. Soc.* **2020**, *142*, 4807−4819.
(4) Li, H.; Paolucci, C.; Khurana, I.; Wilcox, L.; Goltl, F.; Albarracin-Caballero, J. D.; Shih, A. J.; Ribeiro, F. H.; Gounder, R.; Schneider, W. F. Consequences of exchange-site heterogeneity and dynamics on the UV-visible spectrum of Cu-exchanged SSZ-13. *Chem. Sci.* **2019**, *10*, 2373−2384.
(5) Taylor, H. S. A theory of the catalytic surface. *Proc. R. Soc. London, Ser. A* **1925**, *108*, 105−111.
(6) Boudart, M. Turnover Rates in Heterogeneous Catalysis. *Chem. Rev.* **1995**, *95*, 661−666.
(7) Samantaray, M. K.; D'Elia, V.; Pump, E.; Falivene, L.; Harb, M.; Ould Chikh, S.; Cavallo, L.; Basset, J. M. The Comparison between Single Atom Catalysis and Surface Organometallic Catalysis. *Chem. Rev.* **2020**, *120*, 734−813.
(8) Thomas, J. M.; Raja, R.; Lewis, D. W. Single-Site Heterogeneous Catalysts. *Angew. Chem., Int. Ed.* **2005**, *44*, 6456−6482.
(9) Haag, W. O.; Lago, R. M.; Weisz, P. B. The Active-Site of Acidic Aluminosilicate Catalysts. *Nature* **1984**, *309*, 589−591.
(10) Minachev, K. M.; Garanin, V. I.; Isakov, Y. I. Application of Synthetic Zeolites (Molecular Sieves) To Catalysis. *Russ. Chem. Rev.* **1966**, *35*, 903−917.
(11) Parvulescu, V. I.; Grange, P.; Delmon, B. Catalytic removal of NO. *Catal. Today* **1998**, *46*, 233−316.
(12) Seiyama, T.; Arakawa, T.; Matsuda, T.; Takita, Y.; Yamazoe, N. Catalytic Activity of Transition-Metal Ion-Exchanged Y-Zeolites in Reduction of Nitric-Oxide with Ammonia. *J. Catal.* **1977**, *48*, 1−7.
(13) Shelef, M. Selective Catalytic Reduction of NOx with N-Free Reductants. *Chem. Rev.* **1995**, *95*, 209−225.
(14) Kwak, J. H.; Tonkyn, R. G.; Kim, D. H.; Szanyi, J.; Peden, C. H. F. Excellent activity and selectivity of Cu-SSZ-13 in the selective catalytic reduction of NOx with NH_3. *J. Catal.* **2010**, *275*, 187−190.
(15) Paolucci, C.; Di Iorio, J. R.; Ribeiro, F. H.; Gounder, R.; Schneider, W. F. Catalysis Science of NOx Selective Catalytic Reduction With Ammonia Over Cu-SSZ-13 and Cu-SAPO-34. *Adv. Catal.* **2016**, *59*, 1−107.
(16) Chen, H.-Y. Cu/Zeolite SCR Catalysts for Automotive Diesel NOx Emission Control. In *Urea-SCR Technology for deNOx After Treatment of Diesel Exhausts*; Nova, I., Tronconi, E., Eds., Springer: New York, 2014; pp 123−147.
(17) Peden, C. H. F. Cu/Chabazite catalysts for 'Lean-Burn' vehicle emission control. *J. Catal.* **2019**, *373*, 384−389.
(18) Gao, F.; Mei, D. H.; Wang, Y. L.; Szanyi, J.; Peden, C. H. F. Selective Catalytic Reduction over Cu/SSZ-13: Linking Homo- and Heterogeneous Catalysis. *J. Am. Chem. Soc.* **2017**, *139*, 4935−4942.
(19) Verma, A. A.; Bates, S. A.; Anggara, T.; Paolucci, C.; Parekh, A. A.; Kamasamudram, K.; Yezerets, A.; Miller, J. T.; Delgass, W. N.; Schneider, W. F.; Ribeiro, F. H. NO oxidation: A probe reaction on Cu-SSZ-13. *J. Catal.* **2014**, *312*, 179−190.
(20) Bates, S. A.; Verma, A. A.; Paolucci, C.; Parekh, A. A.; Anggara, T.; Yezerets, A.; Schneider, W. F.; Miller, J. T.; Delgass, W. N.; Ribeiro, F. H. Identification of the active Cu site in standard selective catalytic reduction with ammonia on Cu-SSZ-13. *J. Catal.* **2014**, *312*, 87−97.
(21) Li, H.; Paolucci, C.; Schneider, W. F. Zeolite Adsorption Free Energies from ab Initio Potentials of Mean Force. *J. Chem. Theory Comput.* **2018**, *14*, 929−938.
(22) Borfecchia, E.; Lomachenko, K. A.; Giordanino, F.; Falsig, H.; Beato, P.; Soldatov, A. V.; Bordiga, S.; Lamberti, C. Revisiting the nature of Cu sites in the activated Cu-SSZ-13 catalyst for SCR reaction. *Chem. Sci.* **2015**, *6*, 548−563.
(23) Giordanino, F.; Vennestrøm, P. N.; Lundegaard, L. F.; Stappen, F. N.; Mossin, S.; Beato, P.; Bordiga, S.; Lamberti, C. Characterization of Cu-exchanged SSZ-13: a comparative FTIR, UV-Vis, and EPR study with Cu-ZSM-5 and Cu-β with similar Si/Al and Cu/Al ratios. *Dalton Trans.* **2013**, *42*, 12741−12761.
(24) Korhonen, S. T.; Fickel, D. W.; Lobo, R. F.; Weckhuysen, B. M.; Beale, A. M. Isolated Cu^{2+} ions: active sites for selective catalytic reduction of NO. *Chem. Commun.* **2011**, *47*, 800−802.
(25) Di Iorio, J. R.; Bates, S. A.; Verma, A. A.; Delgass, W. N.; Ribeiro, F. H.; Miller, J. T.; Gounder, R. The Dynamic Nature of Brønsted Acid Sites in Cu−Zeolites During NOx Selective Catalytic Reduction: Quantification by Gas-Phase Ammonia Titration. *Top. Catal.* **2015**, *58*, 424−434.
(26) Bates, S. A.; Delgass, W. N.; Ribeiro, F. H.; Miller, J. T.; Gounder, R. Methods for NH_3 titration of Brønsted acid sites in Cu-zeolites that catalyze the selective catalytic reduction of NOx with NH_3. *J. Catal.* **2014**, *312*, 26−36.
(27) Loewenstein, W. The distribution of aluminum in the tetrahedra of silicates and aluminates. *Am. Mineral.* **1954**, *39*, 92−96.
(28) Deimund, M. A.; Harrison, L.; Lunn, J. D.; Liu, Y.; Malek, A.; Shayib, R.; Davis, M. E. Effect of Heteroatom Concentration in SSZ-13 on the Methanol-to-Olefins Reaction. *ACS Catal.* **2016**, *6*, 542−550.
(29) Di Iorio, J. R.; Gounder, R. Controlling the Isolation and Pairing of Aluminum in Chabazite Zeolites Using Mixtures of Organic and Inorganic Structure-Directing Agents. *Chem. Mater.* **2016**, *28*, 2236−2247.
(30) Di Iorio, J. R.; Nimlos, C. T.; Gounder, R. Introducing Catalytic Diversity into Single-Site Chabazite Zeolites of Fixed Composition via Synthetic Control of Active Site Proximity. *ACS Catal.* **2017**, *7*, 6663−6674.
(31) Ipek, B.; Wulfers, M. J.; Kim, H.; Göltl, F.; Hermans, I.; Smith, J. P.; Booksh, K. S.; Brown, C. M.; Lobo, R. F. Formation of $[Cu_2O_2]^{2+}$ and $[Cu_2O]^{2+}$ toward C−H Bond Activation in Cu-SSZ-13 and Cu-SSZ-39. *ACS Catal.* **2017**, *7*, 4291−4303.
(32) Oord, R.; Schmidt, J. E.; Weckhuysen, B. M. Methane-to-methanol conversion over zeolite Cu-SSZ-13, and its comparison with the selective catalytic reduction of NOx with NH_3. *Catal. Sci. Technol.* **2018**, *8*, 1028−1038.
(33) Negri, C.; Borfecchia, E.; Cutini, M.; Lomachenko, K. A.; Janssens, T. V. W.; Berlier, G.; Bordiga, S. Evidence of Mixed-Ligand Complexes in Cu-CHA by Reaction of Cu Nitrates with NO/NH_3 at Low Temperature. *ChemCatChem* **2019**, *11*, 3828−3838.
(34) Negri, C.; Signorile, M.; Porcaro, N. G.; Borfecchia, E.; Berlier, G.; Janssens, T. V. W.; Bordiga, S. Dynamic CuII/CuI speciation in Cu-CHA catalysts by in situ Diffuse Reflectance UV−vis-NIR spectroscopy. *Appl. Catal., A* **2019**, *578*, 1−9.
(35) Wulfers, M. J.; Teketel, S.; Ipek, B.; Lobo, R. F. Conversion of methane to methanol on copper-containing small-pore zeolites and zeotypes. *Chem. Commun.* **2015**, *51*, 4447−4450.
(36) Borfecchia, E.; Pappas, D. K.; Dyballa, M.; Lomachenko, K. A.; Negri, C.; Signorile, M.; Berlier, G. Evolution of active sites during selective oxidation of methane to methanol over Cu-CHA and Cu-MOR zeolites as monitored by operando XAS. *Catal. Today* **2019**, *333*, 17−27.
(37) Pappas, D. K.; Borfecchia, E.; Dyballa, M.; Pankin, I. A.; Lomachenko, K. A.; Martini, A.; Signorile, M.; Teketel, S.; Arstad, B.; Berlier, G.; Lamberti, C.; Bordiga, S.; Olsbye, U.; Lillerud, K. P.; Svelle, S.; Beato, P. Methane to Methanol: Structure Activity Relationships for Cu-CHA. *J. Am. Chem. Soc.* **2017**, *139*, 14961−14975.
(38) Borfecchia, E.; Beato, P.; Svelle, S.; Olsbye, U.; Lamberti, C.; Bordiga, S. Cu-CHA - a model system for applied selective redox catalysis. *Chem. Soc. Rev.* **2018**, *47*, 8097−8133.
(39) Da Costa, P.; Moden, B.; Meitzner, G. D.; Lee, D. K.; Iglesia, E. Spectroscopic and chemical characterization of active and inactive Cu species in NO decomposition catalysts based on Cu-ZSM5. *Phys. Chem. Chem. Phys.* **2002**, *4*, 4590−4601.

(40) Dinh, K. T.; Sullivan, M. M.; Narsimhan, K.; Serna, P.; Meyer, R. J.; Dinca, M.; Roman-Leshkov, Y. Continuous Partial Oxidation of Methane to Methanol Catalyzed by Diffusion-Paired Copper Dimers in Copper-Exchanged Zeolites. *J. Am. Chem. Soc.* **2019**, *141*, 11641−11650.
(41) Giordanino, F.; Borfecchia, E.; Lomachenko, K. A.; Lazzarini, A.; Agostini, G.; Gallo, E.; Soldatov, A. V.; Beato, P.; Bordiga, S.; Lamberti, C. Interaction of NH_3 with Cu-SSZ-13 Catalyst: A Complementary FTIR, XANES, and XES Study. *J. Phys. Chem. Lett.* **2014**, *5*, 1552−1559.
(42) Lomachenko, K. A.; Borfecchia, E.; Negri, C.; Berlier, G.; Lamberti, C.; Beato, P.; Falsig, H.; Bordiga, S. The Cu-CHA deNOx Catalyst in Action: Temperature-Dependent NH_3-Assisted Selective Catalytic Reduction Monitored by Operando XAS and XES. *J. Am. Chem. Soc.* **2016**, *138*, 12025−12028.
(43) Janssens, T. V. W.; Falsig, H.; Lundegaard, L. F.; Vennestrøm, P. N. R.; Rasmussen, S. B.; Moses, P. G.; Giordanino, F.; Borfecchia, E.; Lomachenko, K. A.; Lamberti, C.; Bordiga, S.; Godiksen, A.; Mossin, S.; Beato, P. A Consistent Reaction Scheme for the Selective Catalytic Reduction of Nitrogen Oxides with Ammonia. *ACS Catal.* **2015**, *5*, 2832−2845.
(44) Psofogiannakis, G. M.; McCleerey, J. F.; Jaramillo, E.; van Duin, A. C. T. ReaxFF Reactive Molecular Dynamics Simulation of the Hydration of Cu-SSZ-13 Zeolite and the Formation of Cu Dimers. *J. Phys. Chem. C* **2015**, *119*, 6678−6686.
(45) Krishna, S. H.; Jones, C. B.; Miller, J. T.; Ribeiro, F. H.; Gounder, R. Combined Kinetic and Spectroscopic Interrogation of Cu-Zeolites In Operando: Insights into the Mechanism and Site Requirements of NOx Selective Catalytic Reduction with NH_3. *J. Phys. Chem. Lett.* **2020**, *11* (13), 5029−5036.
(46) Lezcano-Gonzalez, I.; Deka, U.; Arstad, B.; Van Yperen-De Deyne, A.; Hemelsoet, K.; Waroquier, M.; Van Speybroeck, V.; Weckhuysen, B. M.; Beale, A. M. Determining the storage, availability and reactivity of NH_3 within Cu-Chabazite-based Ammonia Selective Catalytic Reduction systems. *Phys. Chem. Chem. Phys.* **2014**, *16*, 1639−1650.
(47) Paolucci, C.; Verma, A. A.; Bates, S. A.; Kispersky, V. F.; Miller, J. T.; Gounder, R.; Delgass, W. N.; Ribeiro, F. H.; Schneider, W. F. Isolation of the Copper Redox Steps in the Standard Selective Catalytic Reduction on Cu-SSZ-13. *Angew. Chem., Int. Ed.* **2014**, *53*, 11828−11833.
(48) Günter, T.; Carvalho, H. W. P.; Doronkin, D. E.; Sheppard, T.; Glatzel, P.; Atkins, A. J.; Rudolph, J.; Jacob, C. R.; Casapu, M.; Grunwaldt, J.-D. Structural snapshots of the SCR reaction mechanism on Cu-SSZ-13. *Chem. Commun.* **2015**, *51*, 9227−9230.
(49) Günter, T.; Doronkin, D. E.; Boubnov, A.; Carvalho, H. W. P.; Casapu, M.; Grunwaldt, J.-D. The SCR of NOx with NH_3 Examined by Novel X-ray Emission and X-ray Absorption Methods. *Top. Catal.* **2016**, *59*, 866−874.
(50) Gomez-Lor, B.; Iglesias, M.; Cascales, C.; Gutierrez-Puebla, E.; Monge, M. A diamine copper (I) complex stabilized in situ within the ferrierite framework. Catalytic properties. *Chem. Mater.* **2001**, *13*, 1364−1368.
(51) Lamble, G.; Moen, A.; Nicholson, D. G. Structure of the diamminecopper (I) ion in solution. An X-ray absorption spectroscopic study. *J. Chem. Soc., Faraday Trans.* **1994**, *90*, 2211−2213.
(52) Jones, C. B.; Khurana, I.; Krishna, S. H.; Shih, A. J.; Delgass, W. N.; Miller, J. T.; Ribeiro, F. H.; Schneider, W. F.; Gounder, R. Effects of Dioxygen Pressure on Rates of NOx Selective Catalytic Reduction with NH_3 on Cu-CHA Zeolites. *J. Catal.* **2020**, *389*, 140−149.
(53) Liu, C.; Kubota, H.; Amada, T.; Kon, K.; Toyao, T.; Maeno, Z.; Ueda, K.; Ohyama, J.; Satsuma, A.; Tanigawa, T.; Tsunoji, N.; Sano, T.; Shimizu, K. In Situ Spectroscopic Studies on the Redox Cycle of NH_3-SCR over Cu-CHA Zeolites. *ChemCatChem* **2020**, *12*, 3050−3059.
(54) Gao, F.; Walter, E. D.; Kollar, M.; Wang, Y.; Szanyi, J.; Peden, C. H. F. Understanding ammonia selective catalytic reduction kinetics over Cu/SSZ-13 from motion of the Cu ions. *J. Catal.* **2014**, *319*, 1−14.
(55) Chen, L.; Jansson, J.; Skoglundh, M.; Gronbeck, H. Mechanism for Solid-State Ion Exchange of Cu+ into Zeolites. *J. Phys. Chem. C* **2016**, *120*, 29182−29189.
(56) Hammershøi, P. S.; Negri, C.; Berlier, G.; Bordiga, S.; Beato, P.; Janssens, T. V. W. Temperature-programmed reduction with NO as a characterization of active Cu in Cu-CHA catalysts for NH_3-SCR. *Catal. Sci. Technol.* **2019**, *9*, 2608−2619.
(57) Villamaina, R.; Liu, S. J.; Nova, I.; Tronconi, E.; Ruggeri, M. P.; Collier, J.; York, A.; Thompsett, D. Speciation of Cu Cations in Cu-CHA Catalysts for NH_3-SCR: Effects of SiO_2/AlO_3 Ratio and Cu-Loading Investigated by Transient Response Methods. *ACS Catal.* **2019**, *9*, 8916−8927.
(58) Villamaina, R.; Iacobone, U.; Nova, I.; Tronconi, E.; Ruggeri, M. P.; Collier, J.; Thompsett, D. Low-T CO oxidation over Cu-CHA catalysts in presence of NH_3: Probing the mobility of Cu^{II} ions and the role of multinuclear Cu^{II} species. *ChemCatChem* **2020**, *12*, 3843−3848.
(59) Goltl, F.; Conrad, S.; Wolf, P.; Muller, P.; Love, A. M.; Burt, S. P.; Wheeler, J. N.; Hamers, R. J.; Hummer, K.; Kresse, G.; Mavrikakis, M.; Hermans, I. UV-Vis and Photoluminescence Spectroscopy to Understand the Coordination of Cu Cations in the Zeolite SSZ-13. *Chem. Mater.* **2019**, *31*, 9582−9592.
(60) Newton, M. A.; Knorpp, A. J.; Sushkevich, V. L.; Palagin, D.; van Bokhoven, J. A. Active sites and mechanisms in the direct conversion of methane to methanol using Cu in zeolitic hosts: a critical examination. *Chem. Soc. Rev.* **2020**, *49*, 1449−1486.
(61) Ravi, M.; Ranocchiari, M.; van Bokhoven, J. A. The Direct Catalytic Oxidation of Methane to Methanol-A Critical Assessment. *Angew. Chem., Int. Ed.* **2017**, *56*, 16464−16483.
(62) Knorpp, A. J.; Newton, M. A.; Mizuno, S. C. M.; Zhu, J.; Mebrate, H.; Pinar, A. B.; van Bokhoven, J. A. Comparative performance of Cu-zeolites in the isothermal conversion of methane to methanol. *Chem. Commun.* **2019**, *55*, 11794−11797.
(63) Sushkevich, V. L.; van Bokhoven, J. A. Methane-to-Methanol: Activity Descriptors in Copper-Exchanged Zeolites for the Rational Design of Materials. *ACS Catal.* **2019**, *9*, 6293−6304.
(64) Knott, B. C.; Nimlos, C. T.; Robichaud, D. J.; Nimlos, M. R.; Kim, S.; Gounder, R. Consideration of the Aluminum Distribution in Zeolites in Theoretical and Experimental Catalysis Research. *ACS Catal.* **2018**, *8*, 770−784.
(65) Li, S. C.; Gounder, R.; Debellis, A.; Muller, I. B.; Prasad, S.; Moini, A.; Schneider, W. F. Influence of the N,N,N-Trimethyl-1-adamantyl Ammonium Structure-Directing Agent on Al Substitution in SSZ-13 Zeolite. *J. Phys. Chem. C* **2019**, *123*, 17454−17458.
(66) Kosinov, N.; Liu, C.; Hensen, E. J. M.; Pidko, E. A. Engineering of Transition Metal Catalysts Confined in Zeolites. *Chem. Mater.* **2018**, *30*, 3177−3198.
(67) Chen, L.; Falsig, H.; Janssens, T. V. W.; Grönbeck, H. Activation of oxygen on $(NH_3CuNH_3)^+$ in NH_3-SCR over Cu-CHA. *J. Catal.* **2018**, *358*, 179−186.
(68) Chen, L.; Falsig, H.; Janssens, T. V. W.; Jansson, J.; Skoglundh, M.; Gronbeck, H. Effect of Al-distribution on oxygen activation over Cu-CHA. *Catal. Sci. Technol.* **2018**, *8*, 2131−2136.
(69) Thirumalai, H.; Rimer, J. D.; Grabow, L. C. Quantification and Statistical Analysis of Errors Related to the Approximate Description of Active Site Models in Metal-Exchanged Zeolites. *ChemCatChem* **2019**, *11*, 5055−5067.
(70) Goncalves, T. J.; Plessow, P. N.; Studt, F. On the Accuracy of Density Functional Theory in Zeolite Catalysis. *ChemCatChem* **2019**, *11*, 4368−4376.
(71) Chen, L.; Janssens, T. V. W.; Gronbeck, H. A comparative test of different density functionals for calculations of NH_3-SCR over Cu-Chabazite. *Phys. Chem. Chem. Phys.* **2019**, *21*, 10923−10930.
(72) Negri, C.; Hammershøi, P. S.; Janssens, T. V. W.; Beato, P.; Berlier, G.; Bordiga, S. Investigating the Low Temperature Formation of Cu^{II}-(N,O) Species on Cu-CHA Zeolites for the Selective Catalytic Reduction of NOx. *Chem. - Eur. J.* **2018**, *24*, 12044−12053.
(73) Greenaway, A. G.; Marberger, A.; Thetford, A.; Lezcano-González, I.; Agote-Arán, M.; Nachtegaal, M.; Ferri, D.; Kröcher, O.; Catlow, C. R. A.; Beale, A. M. Detection of key transient Cu

intermediates in SSZ-13 during NH_3-SCR deNOx by modulation excitation IR spectroscopy. *Chem. Sci.* **2020**, *11*, 447−455.

(74) Chen, P. R.; Khetan, A.; Jablonska, M.; Simbock, J.; Muhler, M.; Palkovits, R.; Pitsch, H.; Simon, U. Local dynamics of copper active sites in zeolite catalysts for selective catalytic reduction of NOx with NH_3. *Appl. Catal., B* **2018**, *237*, 263−272.

(75) Liu, C.; Kubota, H.; Toyao, T.; Maeno, Z.; Shimizu, K.-i. Mechanistic insights into the oxidation of copper(i) species during NH_3-SCR over Cu-CHA zeolites: a DFT study. *Catal. Sci. Technol.* **2020**, *10*, 3586−3593.

(76) Chen, L.; Janssens, T. V. W.; Vennestrøm, P. N. R.; Jansson, J.; Skoglundh, M.; Grönbeck, H. A Complete Multisite Reaction Mechanism for Low-Temperature NH_3-SCR over Cu-CHA. *ACS Catal.* **2020**, *10*, 5646−5656.

(77) Gao, F.; Washton, N. M.; Wang, Y.; Kollár, M.; Szanyi, J.; Peden, C. H. F. Effects of Si/Al ratio on Cu/SSZ-13 NH_3-SCR catalysts: Implications for the active Cu species and the roles of Brønsted acidity. *J. Catal.* **2015**, *331*, 25−38.

(78) Partridge, W. P.; Joshi, S. Y.; Pihl, J. A.; Currier, N. W. New operando method for quantifying the relative half-cycle rates of the NO SCR redox cycle over Cu-exchanged zeolites. *Appl. Catal., B* **2018**, *236*, 195−204.

(79) Kispersky, V. F.; Kropf, A. J.; Ribeiro, F. H.; Miller, J. T. Low absorption vitreous carbon reactors for operando XAS: a case study on Cu/Zeolites for selective catalytic reduction of NO(x) by NH_3. *Phys. Chem. Chem. Phys.* **2012**, *14*, 2229−2238.

(80) Ueda, K.; Ohyama, J.; Satsuma, A. In Situ XAFS Study of Dynamic Behavior of Cu Species in MFI-Zeolite under Element Gases of Ammonia Selective Catalytic Reduction. *Chem. Lett.* **2017**, *46*, 1390−1392.

(81) Ye, Q.; Wang, L.; Yang, R. T. Activity, propene poisoning resistance and hydrothermal stability of copper exchanged chabazite-like zeolite catalysts for SCR of NO with ammonia in comparison to Cu/ZSM-5. *Appl. Catal., A* **2012**, *427−428*, 24−34.

(82) Kwak, J. H.; Zhu, H.; Lee, J. H.; Peden, C. H. F.; Szanyi, J. Two different cationic positions in Cu-SSZ-13? *Chem. Commun.* **2012**, *48*, 4758−4760.

(83) Gao, F.; Kwak, J. H.; Szanyi, J.; Peden, C. H. F. Current Understanding of Cu-Exchanged Chabazite Molecular Sieves for Use as Commercial Diesel Engine DeNOx Catalysts. *Top. Catal.* **2013**, *56*, 1441−1459.

(84) Chen, L.; Janssens, T. V. W.; Skoglundh, M.; Gronbeck, H. Interpretation of NH3-TPD Profiles from Cu-CHA Using First-Principles Calculations. *Top. Catal.* **2019**, *62*, 93−99.

(85) Fahami, A. R.; Gunter, T.; Doronkin, D. E.; Casapu, M.; Zengel, D.; Vuong, T. H.; Simon, M.; Breher, F.; Kucherov, A. V.; Bruckner, A.; Grunwaldt, J. D. The dynamic nature of Cu sites in Cu-SSZ-13 and the origin of the seagull NOx conversion profile during NH_3-SCR. *React. Chem. Eng.* **2019**, *4*, 1000−1018.

(86) Marberger, A.; Petrov, A. W.; Steiger, P.; Elsener, M.; Krocher, O.; Nachtegaal, M.; Ferri, D. Time-resolved copper speciation during selective catalytic reduction of NO on Cu-SSZ-13. *Nat. Catal.* **2018**, *1*, 221−227.

(87) Kerkeni, B.; Berthout, D.; Berthomieu, D.; Doronkin, D. E.; Casapu, M.; Grunwaldt, J. D.; Chizallet, C. Copper Coordination to Water and Ammonia in Cu-II-Exchanged SSZ-13: Atomistic Insights from DFT Calculations and in Situ XAS Experiments. *J. Phys. Chem. C* **2018**, *122*, 16741−16755.

(88) Borfecchia, E.; Negri, C.; Lomachenko, K. A.; Lamberti, C.; Janssens, T. V. W.; Berlier, G. Temperature-dependent dynamics of NH_3-derived Cu species in the Cu-CHA SCR catalyst. *React. Chem. Eng.* **2019**, *4*, 1067−1080.

(89) Vennestrom, P. N. R.; Lundegaard, L. F.; Tyrsted, C.; Bokarev, D. A.; Mytareva, A. I.; Baeva, G. N.; Stakheev, A. Y.; Janssens, T. V. W. The Role of Protons and Formation $Cu(NH_3)_2^+$ During Ammonia-Assisted Solid-State Ion Exchange of Copper(I) Oxide into Zeolites. *Top. Catal.* **2019**, *62*, 100−107.

(90) Shwan, S.; Skoglundh, M.; Lundegaard, L. F.; Tiruvalam, R. R.; Janssens, T. V. W.; Carlsson, A.; Vennestrom, P. N. R. Solid-State Ion-Exchange of Copper into Zeolites Facilitated by Ammonia at Low Temperature. *ACS Catal.* **2015**, *5*, 16−19.

(91) Daya, R.; Joshi, S. Y.; Luo, J. Y.; Dadi, R. K.; Currier, N. W.; Yezerets, A. On kinetic modeling of change in active sites upon hydrothermal aging of Cu-SSZ-13. *Appl. Catal., B* **2020**, *263*, 118368.

(92) Woo, J.; Bernin, D.; Ahari, H.; Shost, M.; Zammit, M.; Olsson, L. Regeneration of water-deactivated Cu/SAPO-34(MO) with acids. *Catal. Sci. Technol.* **2020**, *10*, 1539−1550.

(93) Woo, J.; Bernin, D.; Ahari, H.; Shost, M.; Zammit, M.; Olsson, L. Understanding the mechanism of low temperature deactivation of Cu/SAPO-34 exposed to various amounts of water vapor in the NH_3-SCR reaction. *Catal. Sci. Technol.* **2019**, *9*, 3623−3636.

(94) Wang, A. Y.; Chen, Y.; Walter, E. D.; Washton, N. M.; Mei, D. H.; Varga, T.; Wang, Y. L.; Szanyi, J.; Wang, Y.; Peden, C. H. F.; Gao, F. Unraveling the mysterious failure of Cu/SAPO-34 selective catalytic reduction catalysts. *Nat. Commun.* **2019**, *10*, 1137.

(95) Leistner, K.; Olsson, L. Deactivation of Cu/SAPO-34 during low-temperature NH3-SCR. *Appl. Catal., B* **2015**, *165*, 192−199.

(96) Piccini, G.; Alessio, M.; Sauer, J. Ab Initio Calculation of Rate Constants for Molecule−Surface Reactions with Chemical Accuracy. *Angew. Chem., Int. Ed.* **2016**, *55*, 5235−5237.

(97) Jorgensen, M.; Chen, L.; Gronbeck, H. Monte Carlo Potential Energy Sampling for Molecular Entropy in Zeolites. *J. Phys. Chem. C* **2018**, *122*, 20351−20357.

(98) Jorgensen, M.; Gronbeck, H. Adsorbate Entropies with Complete Potential Energy Sampling in Microkinetic Modeling. *J. Phys. Chem. C* **2017**, *121*, 7199−7207.

(99) Dauenhauer, P. J.; Abdelrahman, O. A. A Universal Descriptor for the Entropy of Adsorbed Molecules in Confined Spaces. *ACS Cent. Sci.* **2018**, *4*, 1235−1243.

(100) Barducci, A.; Bonomi, M.; Parrinello, M. Metadynamics. *Wiley Interdiscip. Rev.: Comput. Mol. Sci.* **2011**, *1*, 826−843.

(101) De Wispelaere, K.; Ensing, B.; Ghysels, A.; Meijer, E. J.; Van Speybroeck, V. Complex Reaction Environments and Competing Reaction Mechanisms in Zeolite Catalysis: Insights from Advanced Molecular Dynamics. *Chem. - Eur. J.* **2015**, *21*, 9385−9396.

(102) Li, G. N.; Pidko, E. A. The Nature and Catalytic Function of Cation Sites in Zeolites: a Computational Perspective. *ChemCatChem* **2019**, *11*, 134−156.

(103) Li, S. C.; Zheng, Y.; Gao, F.; Szanyi, J.; Schneider, W. F. Experimental and Computational Interrogation of Fast SCR Mechanism and Active Sites on H-Form SSZ-13. *ACS Catal.* **2017**, *7*, 5087−5096.

(104) Brogaard, R. Y.; Komurcu, M.; Dyballa, M. M.; Botan, A.; Van Speybroeck, V.; Olsbye, U.; De Wispelaere, K. Ethene Dimerization on Zeolite-Hosted Ni Ions: Reversible Mobilization of the Active Site. *ACS Catal.* **2019**, *9*, 5645−5650.

(105) Li, S. C.; Wang, Y. J.; Wu, T.; Schneider, W. F. First-Principles Analysis of Site- and Condition-Dependent Fe Speciation in SSZ-13 and Implications for Catalyst Optimization. *ACS Catal.* **2018**, *8*, 10119−10130.

(106) Imbao, J.; van Bokhoven, J. A.; Clark, A.; Nachtegaal, M. Elucidating the mechanism of heterogeneous Wacker oxidation over Pd-Cu/zeolite Y by transient XAS. *Nat. Commun.* **2020**, *11*, 1118.

(107) Shibata, J.; Shimizu, K.; Takada, Y.; Shichi, A.; Yoshida, H.; Satokawa, S.; Satsuma, A.; Hattori, T. Structure of active Ag clusters in Ag zeolites for SCR of NO by propane in the presence of hydrogen. *J. Catal.* **2004**, *227*, 367−374.

Supporting Information

Solvation and Mobilization of Copper Active Sites in Zeolites by Ammonia: Consequences for the Catalytic Reduction of Nitrogen Oxides

Christopher Paolucci,[‖] *John R. Di Iorio,*[§,†] *William F. Schneider,*[*,#] *and Rajamani Gounder*[*,§]

[‖]Department of Chemical Engineering, University of Virginia, Charlottesville, VA 22903 (USA)

[§]Charles D. Davidson School of Chemical Engineering, Purdue University, West Lafayette, IN 47907 (USA)

[#]Department of Chemical and Biomolecular Engineering, University of Notre Dame, Notre Dame, IN 46556 (USA)

*Corresponding author e-mail addresses: rgounder@purdue.edu, wschneider@nd.edu

S2.1 NH_3-SCR and Dry NO Oxidation Rates

Table S1. NH_3-SCR kinetic parameters measured on a series of Cu-CHA samples with Si/Al = 15 and Cu/Al varying from 0.03-0.44. Data corresponding to Figure 2a (main text). Adapted with permission from ref. 1. Copyright 2017 American Association for the Advancement of Science.

Si/Al	Cu/Al	Cu /1000Å^3	SCR Rate (10^{-3} mol NO/mol Cu/s)	SCR Rate (10^{-3} NO/1000Å^3/s)	O_2 order[a]	E_{app}[b]
15	0.03	0.03	1.8	0.05	0.8	47
15	0.08	0.07	2.3	0.16	0.7	50
15	0.10	0.09	3.3	0.30	0.7	56
15	0.12	0.11	4.5	0.50	0.7	56
15	0.19	0.18	6.5	1.17	0.5	60
15	0.25	0.23	7.8	1.79	0.4	63
15	0.37	0.35	7.4	2.59	0.4	66
15	0.44	0.41	7.8	3.20	0.3	74

[a]Errors are ± 0.1.
[b]Errors are ± 7 kJ/mol.

Table S2. NH_3-SCR kinetic parameters and dry NO oxidation rates measured on a series of Cu-exchanged SSZ-13 samples with Si/Al = 4.3-4.5 and Cu/Al varying from 0.02-0.39; arranged by increasing Cu/Al). Data corresponding to Figure 2b (main text). Adapted with permission from refs. 2,3. Copyright 2014 Elsevier.

Si/Al	Cu/Al	Cu /1000Å^3	SCR Rate (10^{-3} NO/1000Å^3/s)	SCR O_2 order[a]	SCR E_{app}[b]	Dry NO Oxidation Rate (10^{-4} NO/1000Å^3/s)
4.3	0.02	0.06	0.2	0.5	42	0
4.3	0.04	0.11	1.5	0.5	68	0
4.5	0.09	0.25	1.8	0.3	64	0
4.5	0.16	0.44	2.8	0.3	70	0
4.5	0.20	0.55	3.6	0.3	71	0
4.5	0.31	0.85	n.m.	n.m.	n.m.	0.5
4.5	0.35	0.96	2.9	0.2	71	1.3
4.5	0.39	1.07	n.m.	n.m.	n.m.	1.6

[a]Errors are ± 0.1.
[b]Errors are ± 5 kJ/mol.
n.m. not measured

S3.1 Energies of Cu species at 1Al and 2Al sites

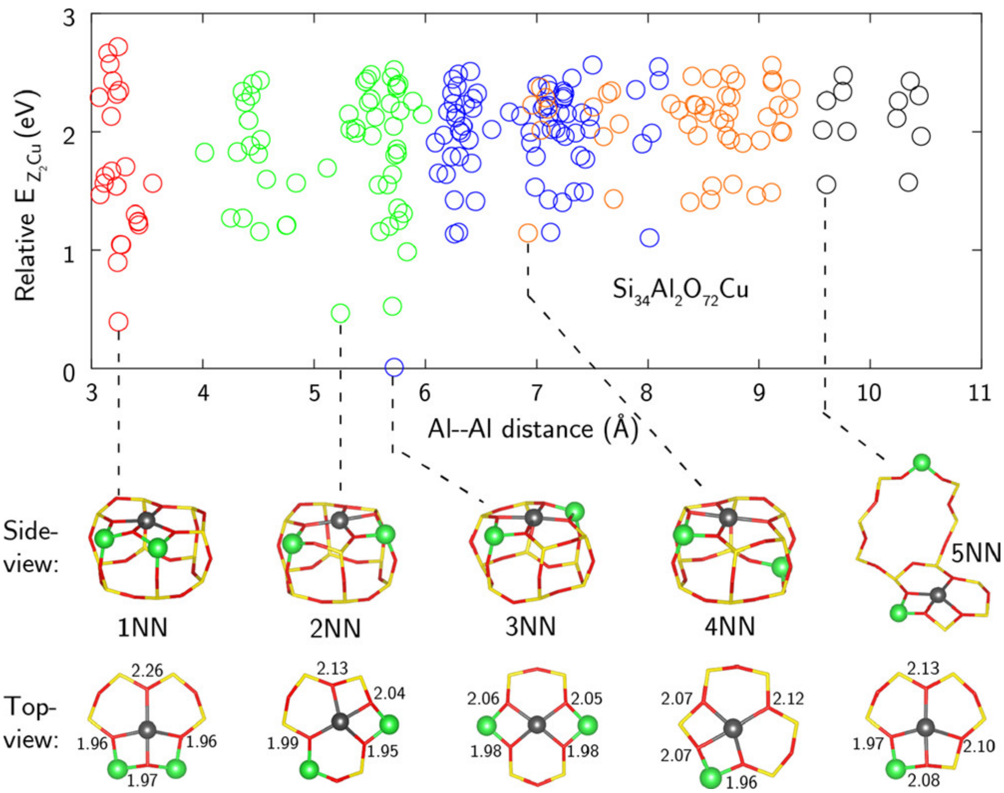

Figure S1. Z_2Cu energy vs Al–Al lattice separation, relative to the lowest energy structure (3NN 6-MR). Symbol color indicates connectivity distance: red–1NN, green–2NN, blue–3NN, orange–4NN, black–5NN. Lowest-energy structures and corresponding Cu–O_f distances (in Å) at each connectivity distance are shown. Atom colors: yellow–Si, green–Al, red–O, pink–H. Reproduced from ref. 4. Copyright 2018 American Chemical Society.

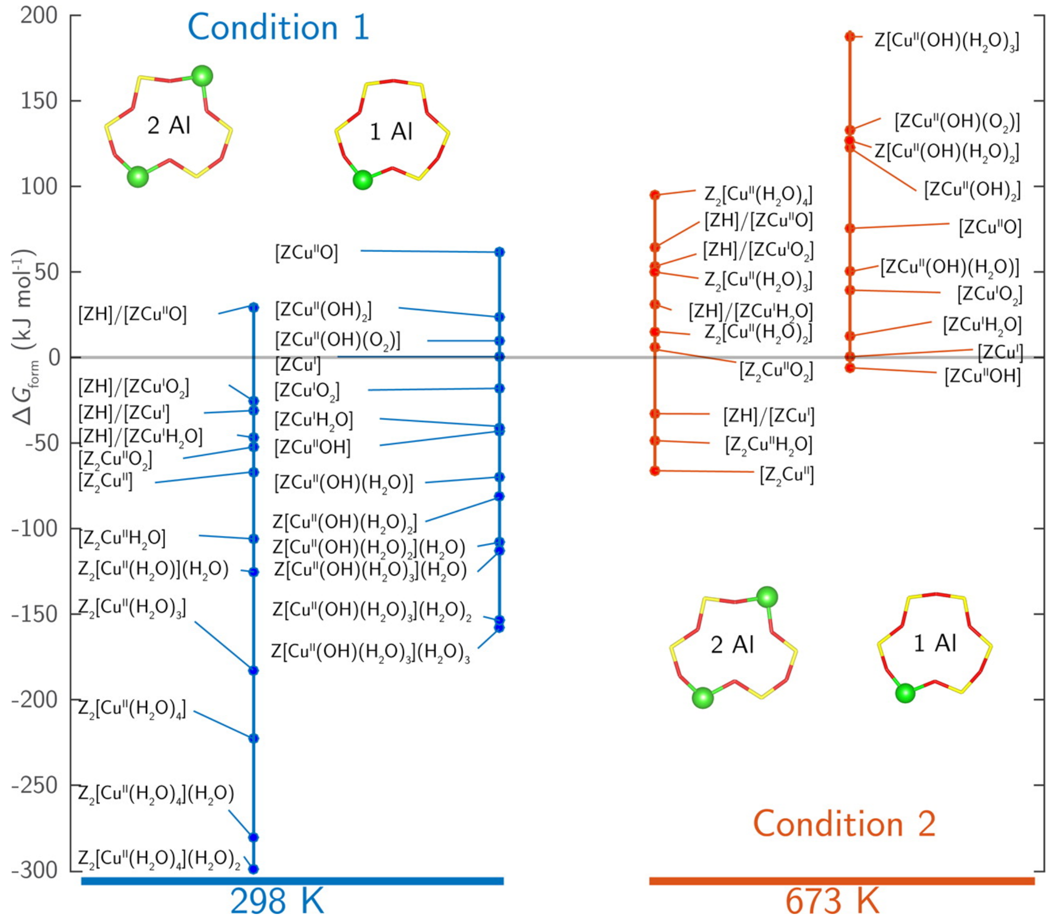

Figure S2. Formation free energies (ΔG_{form}) CuH_xO_y species at (left) 298 K, 2 kPa H_2O, 20 kPa O_2, and at (right) 673 K, 2 kPa H_2O, 20 kPa O_2 on the 2Al (Z_2Cu) and 1Al (ZCu) sites. Common energy reference set through Eq. (S1). Reproduced from ref. 5. Copyright 2016 American Chemical Society.

$$[Z_2CuH_2O] + [ZH] \rightarrow [ZH]/[ZH] + [ZCuOH] \quad ; \quad \Delta E = +66 \text{ kJ/mol} \tag{S1}$$

S3.2 Composition of Synthesized Cu-CHA Materials

Table S3. Bulk elemental analysis and fraction of isolated Cu^{2+} and $Cu^{2+}(OH)$ sites on a series of Cu-CHA samples with varying Si/Al (4.5-25) and Cu/Al (0.03-0.59); arranged by increasing Cu/Al for a fixed Si/Al ratio. Adapted with permission from ref. 1. Copyright 2017 American Association for the Advancement of Science. Adapted from ref. 5. Copyright 2016 American Chemical Society.

Si/Al	Cu/Al	Cu /1000Å^3	H^+/Al (H-form)	H^+/Al (Cu-form)	$ZCu^{2+}OH/Al^a$	Z_2Cu^{2+}/Al^a
4.5	0.08	0.22	0.46	0.31	0	0.08
4.5	0.21	0.57	0.87	0.42	0	0.21
15	0.03	0.03	0.98	0.93	0	0.03
15	0.08	0.07	0.98	0.81	0	0.08
15	0.10	0.09	0.98	0.80	0.01	0.09
15	0.12	0.11	0.98	0.73	0.03	0.09
15	0.19	0.18	0.98	0.68	0.10	0.09
15	0.25	0.23	1.00	0.64	0.16	0.09
15	0.37	0.35	0.98	0.58	0.28	0.09
15	0.44	0.41	0.98	0.51	0.35	0.09
25	0.21	0.11	0.98	0.74	0.17	0.04
25	0.42	0.24	0.98	0.58	0.37	0.04
25	0.59	0.34	0.98	0.47	0.55	0.04

[a]Determined from titration of residual H^+ sites by NH_3 and thermodynamic preferences for Z_2Cu^{2+} and $ZCu^{2+}OH$ siting.[6,7]

Titrimetric methods were developed to quantify speciation between Z_2Cu and ZCuOH site motifs, given that the former Cu sites exchange 2 H^+ and the latter exchange only 1 H^+. NH_3 is among the only probe bases that can fully access the microporous voids of small-pore CHA zeolites, but it adsorbs strongly on both H^+ and Cu sites and more weakly in various physisorbed states, complicating efforts to distinguish individual site types. However, NH_3 saturation followed by H_2O purge treatments selectively retain only NH_4^+ species, enabling quantifying residual H^+ sites after Cu exchange.[6,7] Cu-CHA materials expected to contain predominantly Z_2Cu or ZCuOH reveal two stoichiometric regimes (Fig. S3), corresponding to exchange of 2 or 1 H^+ with increasing Cu^{2+} content, consistent with the preferential population of Z_2Cu before

ZCuOH sites (Fig. S2). In contrast, Co^{2+} exchanges only as Z_2Co and enumerates 2Al sites (Fig. S3), and thus titrate the same set of proximal Al as Z_2Cu.[5,8]

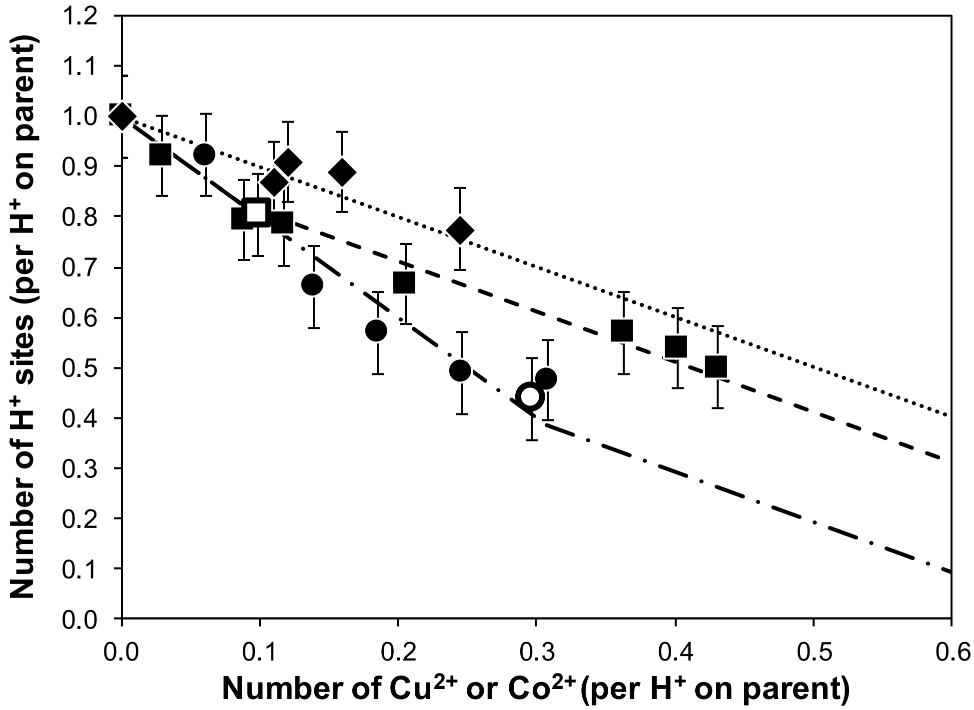

Figure S3. Number of residual H^+ sites after Cu^{2+} (solid) or Co^{2+} (open) exchange (measured by NH_3 titration) with increasing M^{2+} exchange on CHA zeolites synthesized via FAU-to-CHA interconversion (circles, Si/Al = 5), using an equimolar mixture of Na^+ and $TMAda^+$ (squares, Si/Al = 15), and using only $TMAda^+$ (diamonds, Si/Al = 15). Dotted, dashed, and dot-dash lines are predicted Cu^{2+} exchange stoichiometry based on the different synthetic procedures. Reproduced from ref. 5. Copyright 2016 American Chemical Society. Reproduced from ref. 9. Copyright 2017 American Chemical Society.

S7.1 Kinetic models for the transient oxidation experiments

The following equation (a detailed derivation can be found in ref.[1]) was used to model the transient oxidation of Cu^+ in O_2-assisted oxidation XAS experiments:

$$\mathrm{Cu^I\ Fraction} = \frac{[\mathrm{Cu^I}(t)]}{[\mathrm{Cu^I}]_0} = \frac{1 - [\mathrm{Cu^I}]_\infty/[\mathrm{Cu^I}]_0}{1 + 2k\left([\mathrm{Cu^I}]_0 - [\mathrm{Cu^I}]_\infty\right)t} + \frac{[\mathrm{Cu^I}]_\infty}{[\mathrm{Cu^I}]_0} \tag{S2}$$

where Cu^I Fraction is the time-dependent Cu^I concentration divided by the initial Cu^I concentration ($[Cu^I]_0$), k is a pseudo-second-order rate constant, and $[Cu^I]_\infty$ is the unoxidizable, recalcitrant fraction of Cu^I at the end of the transient experiment.

Table S4. Apparent rate constants (k), recalcitrant $[Cu^+]_\infty$/ $[Cu^+]_0$ fractions, and goodness of fit (R^2) to equation S2 for the data corresponding to Figure 8. Adapted with permission from ref. 1. Copyright 2017 American Association for the Advancement of Science.

	0.07 Cu/1000 Å^3	0.22 Cu/1000 Å^3	0.57 Cu/1000 Å^3
k(m^3 mol Cu^{-1}s^{-1})	0.00011	0.00017	0.00082
$[Cu^+]_\infty$/ $[Cu^+]_0$	0.26	0.10	0.05
R^2	0.99	0.98	0.99

S7.2 Predicted recalcitrant Cu^+ fractions from stochastic simulations

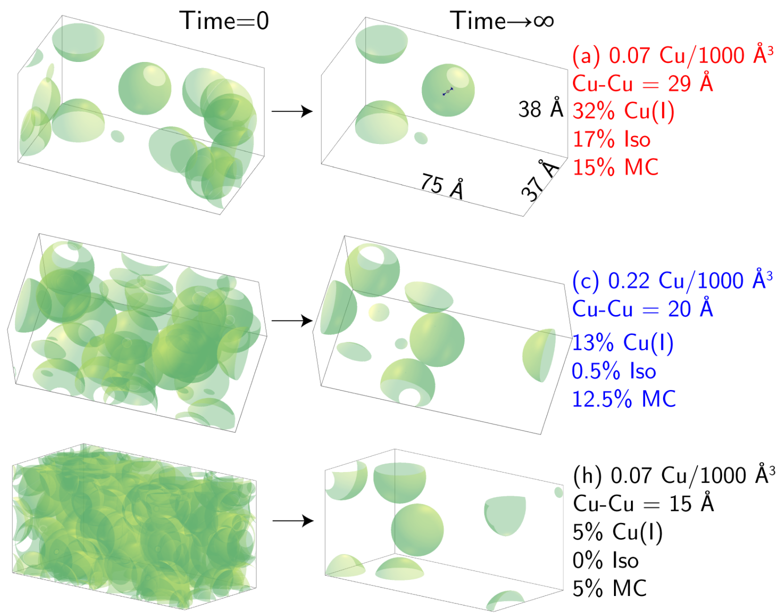

Figure S4. Snapshots taken from stochastic simulations at initial (time = 0) and final (time→∞) Cu^+ spatial distributions corresponding to the three samples in Figure 8. Cu^+ volumetric footprints are denoted by 9 Å–radius green spheres. Simulation results include decomposition of unoxidized Cu^+ fraction into physically isolated (Iso) and functionally isolated (MC) components. Reproduced with permission from ref. 1. Copyright 2017 American Association for the Advancement of Science.

S7.3 Metadynamics simulation of $Cu^{+}(NH_3)_2$ intercage diffusion

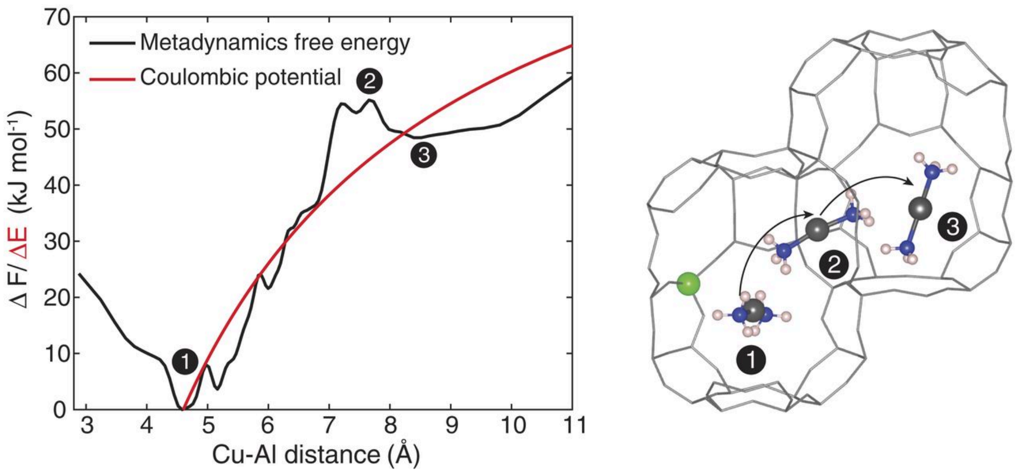

Figure S5. On left, the metadynamics-computed free energy at 473 K of $Cu^{+}(NH_3)_2$ in the 72–T site CHA supercell versus Cu-Al distance. The red line is the energy profile predicted from a point-charge electrostatic model, described in SM section S9. Labeled are reactant state (1) [$Cu^{+}(NH_3)_2$ in the same cage as Al], transition state (2) [$Cu^{+}(NH_3)_2$ diffusion through 8-MR], and product state (3) [$Cu^{+}(NH_3)_2$ in the neighboring cage without Al]. Corresponding representative $Cu^{+}(NH_3)_2$ configurations from the trajectories are shown on the right. Gray, Cu; green, Al; blue, N; and white, H. Reproduced with permission from ref. 1. Copyright 2017 American Association for the Advancement of Science.

S7.4 Both Cu^+ oxidation and Cu^{2+} reduction steps are kinetically relevant during "standard" SCR

SCR rates measured at low (1 kPa) O_2 pressures on Cu-CHA increase quadratically with Cu density in the entire range of Cu densities studied (Fig. S6a), because such conditions cause Cu^+ oxidation rates to become the dominant rate-limiting step (Fig. S6b). These data demonstrate that O_2-assisted oxidation steps prevail in all Cu-CHA zeolites,[10] and that the kinetic relevance of oxidation half-cycle rates to overall SCR rates depends on both Cu density and O_2 partial pressure.

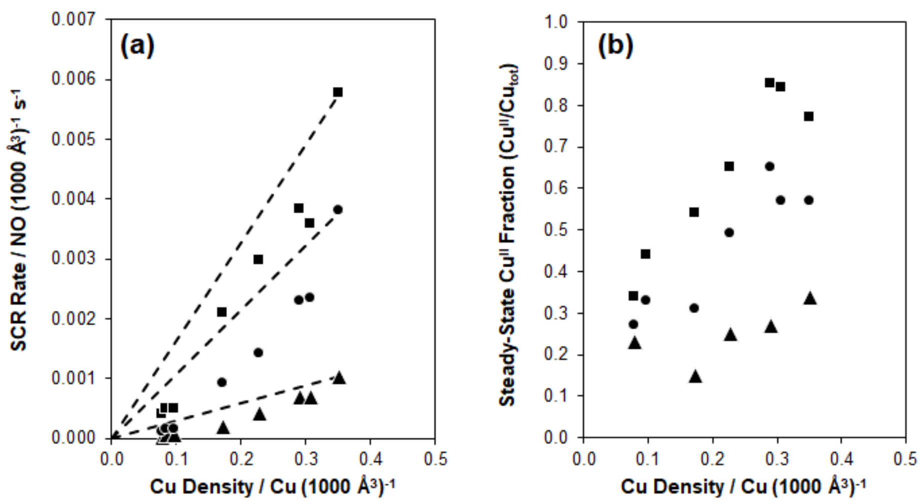

Figure S6. A) SCR rates (per 10^3 $Å^3$, 473 K) measured on Cu-CHA samples at 1 (▲), 10 (●), and 60 kPa (■) O_2 (other reaction conditions: 0.030 kPa NO, 0.030 kPa NH_3, 7 kPa CO_2, 1 kPa H_2O, balance N_2). Dashed lines are drawn through the origin and the rate on highest Cu content sample for each data series to guide the eye, illustrating that SCR rates deviate from a first-order dependence at dilute Cu density. B) Steady-state Cu^+ fraction (Cu^+/Cu_{tot}) at 1 (▲), 10 (●), and 60 kPa O_2 (■) measured *in operando* by XAS as a function of Cu density. Reproduced with permission from ref. 10. Copyright 2020 Elsevier.

REFERENCES

(1) Paolucci, C.; Khurana, I.; Parekh, A. A.; Li, S.; Shih, A. J.; Li, H.; Di Iorio, J. R.; Albarracin-Caballero, J. D.; Yezerets, A.; Miller, J. T.; Delgass, W. N.; Ribeiro, F. H.; Schneider, W. F.; Gounder, R. Dynamic multinuclear sites formed by mobilized copper ions in NOx selective catalytic reduction. *Science* **2017**, *357*, 898-903.

(2) Verma, A. A.; Bates, S. A.; Anggara, T.; Paolucci, C.; Parekh, A. A.; Kamasamudram, K.; Yezerets, A.; Miller, J. T.; Delgass, W. N.; Schneider, W. F.; Ribeiro, F. H. NO oxidation: A probe reaction on Cu-SSZ-13. *J. Catal.* **2014**, *312*, 179-190.

(3) Bates, S. A.; Verma, A. A.; Paolucci, C.; Parekh, A. A.; Anggara, T.; Yezerets, A.; Schneider, W. F.; Miller, J. T.; Delgass, W. N.; Ribeiro, F. H. Identification of the active Cu site in standard selective catalytic reduction with ammonia on Cu-SSZ-13. *J. Catal.* **2014**, *312*, 87-97.

(4) Li, S. C.; Li, H.; Gounder, R.; Debellis, A.; Mueller, I. B.; Prasad, S.; Moini, A.; Schneider, W. F. First-Principles Comparison of Proton and Divalent Copper Cation Exchange Energy Landscapes in SSZ-13 Zeolite. *J. Phys. Chem. C* **2018**, *122*, 23564-23573.

(5) Paolucci, C.; Parekh, A. A.; Khurana, I.; Di Iorio, J. R.; Li, H.; Caballero, J. D. A.; Shih, A. J.; Anggara, T.; Delgass, W. N.; Miller, J. T.; Ribeiro, F. H.; Gounder, R.; Schneider, W. F. Catalysis in a Cage: Condition-Dependent Speciation and Dynamics of Exchanged Cu Cations in SSZ-13 Zeolites. *J. Am. Chem. Soc.* **2016**, *138*, 6028-6048.

(6) Di Iorio, J. R.; Bates, S. A.; Verma, A. A.; Delgass, W. N.; Ribeiro, F. H.; Miller, J. T.; Gounder, R. The Dynamic Nature of Brønsted Acid Sites in Cu–Zeolites During NOx Selective Catalytic Reduction: Quantification by Gas-Phase Ammonia Titration. *Top. Catal.* **2015**, *58*, 424-434.

(7) Bates, S. A.; Delgass, W. N.; Ribeiro, F. H.; Miller, J. T.; Gounder, R. Methods for NH_3 titration of Brønsted acid sites in Cu-zeolites that catalyze the selective catalytic reduction of NOx with NH_3. *J. Catal.* **2014**, *312*, 26-36.

(8) Di Iorio, J. R.; Gounder, R. Controlling the Isolation and Pairing of Aluminum in Chabazite Zeolites Using Mixtures of Organic and Inorganic Structure-Directing Agents. *Chem. Mater.* **2016**, *28*, 2236-2247.

(9) Di Iorio, J. R.; Nimlos, C. T.; Gounder, R. Introducing Catalytic Diversity into Single-Site Chabazite Zeolites of Fixed Composition via Synthetic Control of Active Site Proximity. *ACS Catal.* **2017**, *7*, 6663-6674.

(10) Jones, C. B.; Khurana, I.; Krishna, S. H.; Shih, A. J.; Delgass, W. N.; Miller, J. T.; Ribeiro, F. H.; Schneider, W. F.; Gounder, R. Effects of Dioxygen Pressure on Rates of NOx Selective Catalytic Reduction with NH_3 on Cu-CHA Zeolites. *J. Catal.* **2020**, *389*, 140-149.